

# Resonance phenomena in a nonlinear neuronal circuit

M. Bordet, S. Morfu<sup>†</sup>, and P. Marquié

<sup>1,2,3</sup> Université de Bourgogne - Laboratoire LE2i UMR CNRS 6306, France.  
(E-mail<sup>†</sup>: [smorfu@u-bourgogne.fr](mailto:smorfu@u-bourgogne.fr))

**Abstract.** We characterize a nonlinear circuit driven by a bichromatic excitation, that is the sum of two sinusoidal waves with different frequencies  $f_1$  and  $f_2$  such that  $f_2 > f_1$ . Our experiments are confirmed by a numerical analysis of the system response obtained by solving numerically the differential equations which rule the circuit voltages. Especially, we highlight that the response of the system at the low frequency can be optimized by the amplitude of the high frequency component. By revisiting this well known vibrational resonance effect in the whole amplitude-frequency parametric plane, we show experimentally and numerically that a much better resonance can be achieved when the two frequencies which drive the circuit are multiple or submultiple.

**Keywords:** Nonlinear stochastic systems, Ghost Stochastic Resonance, Vibrational Resonance, Nonlinear electronic circuits..

## 1 Introduction

During the past decades, a great interest has been devoted to the study of the response of the FitzHugh-Nagumo model submitted to different kind of excitations. Depending on the stimuli which drives the system, various resonances have been shown [1–3] such as coherence resonance when the system is only excited by noise [4,5] or Ghost stochastic resonance when noise added to a bichromatic signal drive the system [6,7]. These resonances have allowed to explain a variety of behaviors in nature. This is especially the case in the context of neurosciences, where Coherence Resonance has provided a better understanding of the activity of neurons in absence of stimuli. On the other hand, the way that sensory neurons behave to perceive complex sound have been also fairly good described by the ghost Stochastic Resonance effect [8]. In this communication, the response of a nonlinear circuit whose voltages obey to the classical FitzHugh-Nagumo equations is investigated [9]. More precisely, we focus our interest on the system response to a deterministic bichromatic signal, that is when the sum of two sinusoidal components of different frequencies drive the circuit. To highlight the resonant behaviour of the system, we perform a spectral analysis versus both the amplitude of the high frequency component and the ratio between the low and high frequency drivings. The originality of

---

<sup>8<sup>th</sup></sup> CHAOS Conference Proceedings, 26-29 May 2015, Henri Poincaré Institute, Paris France



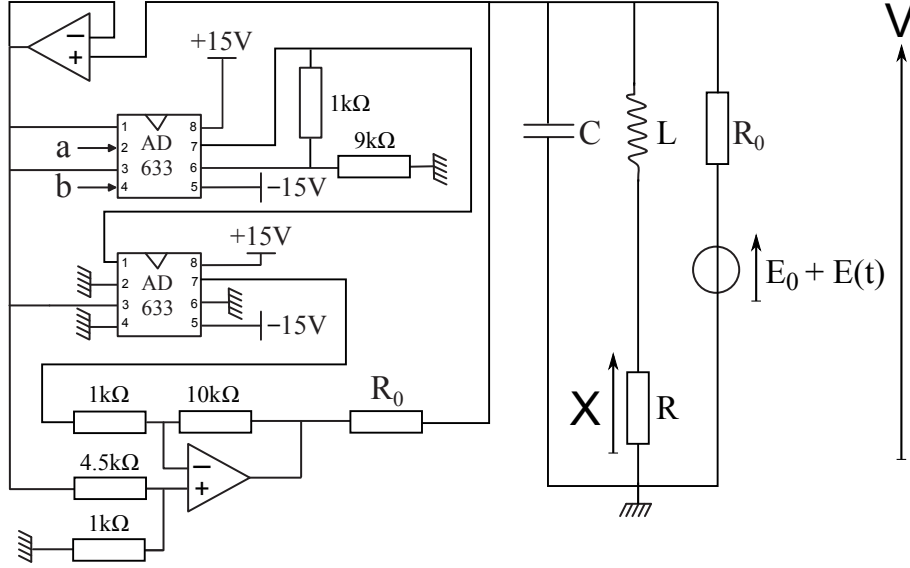


**Fig. 1.** The nonlinear circuit under investigation. The parameters are  $a = 2V$ ,  $b = -2.6V$ ,  $E_0 = -1V$ . Moreover,  $\gamma = 0.24$  and  $\epsilon = 4.249$  are adjusted with the component values  $R_0$ ,  $R$ ,  $L$  and  $C$  via the transformation (4).

our approach is to enable a direct comparison between experiments carried out with our electrical circuit and a numerical study realized by integrating the set of FitzHugh-Nagumo equations. We first present our experimental device and its set-up. Next, we analyze the system response to a bi-chromatic excitation of frequencies  $f_1$  and  $f_2$ . Especially, we consider the high frequency driving as a perturbation which is used to enhance the detection of the low frequency excitation.

## 2 Experimental Device description

In this section, we briefly describe the FitzHugh-Nagumo circuit of fig. 1 whose response has been widely investigated. This circuit has been developed with classical TL081 Amplifiers, AD633JN analog multipliers, a capacitor  $C$ , an inductor  $L$  and linear resistors  $R$  and  $R_0$ . Using Kirchoff laws and the datasheet of the analog multipliers, it can be shown that the voltages  $V$  and  $X$  of this circuit are ruled by the following set of differential equations:

$$\begin{aligned} R_0 C \frac{dV}{dt} &= -V(V - a)(V - b) - \frac{R_0 X}{R} + E_0 + E(t), \\ \frac{L}{R} \frac{dX}{dt} &= V - X. \end{aligned} \quad (1)$$

where  $E_0$  is a constant offset voltage and  $t$  corresponds to the time. Moreover,  $E(t)$  represents the signal which drives the circuit.

Note that, to obtain the normalized FitzHugh-Nagumo set of equations, we can define the normalized time  $\tau$  and the variable  $W$  with the following expressions

$$\tau = \frac{t}{R_0 C}, W = \frac{R_0 \cdot X}{R}. \quad (2)$$

Indeed, using eq. (2) leads to

$$\begin{aligned} \frac{dV}{d\tau} &= -V(V - a)(V - b) - W + E_0 + E(\tau), \\ \frac{dW}{d\tau} &= \epsilon(V - \gamma W), \end{aligned} \quad (3)$$

where the parameters  $\epsilon$  and  $\gamma$  are set with the component values according to the following formula:

$$\epsilon = \frac{R_0^2 C}{L} \quad \text{and} \quad \gamma = \frac{R}{R_0}. \quad (4)$$

In this communication, we will analyze the dynamics of the voltage  $V$  whose shape is appropriate in neuronal context since it represents spikes. In all our experiments, the roots of the cubic nonlinearity will be set by external constant voltage sources to  $a = 2 \text{ Volt}$  and  $b = -2.6 \text{ Volt}$ . Moreover, the component values will be chosen such that  $\gamma = 0.24$  and  $\epsilon = 4.249$ . The constant offset  $E_0$  will be tuned to ensure that the FitzHugh-Nagumo circuit will remain in the excitable state when there is no excitation, that is when  $E(t) = 0$ . In all the following, the value  $E_0 = -1V$  will be considered such that no spikes are triggered in absence of any excitation ( $E(t) = 0$ ).

Lastly, the circuit will be excited with a signal  $E(t)$  obtained by summing two sinusoidal components of low frequency  $f_1$  and high frequency  $f_2$ , but with different amplitudes  $A$  and  $B$ . Thus, using experimental time units, the excitation writes :

$$E(t) = A \cos(2\pi f_1 t) + B \cos(2\pi f_2 t). \quad (5)$$

The amplitude  $A$  of the first sinusoidal component is chosen such that the circuit does not trigger spikes when the second sinusoidal component is not applied, that is when  $B = 0$ . Under this condition, the low frequency component is subthreshold. Throughout this paper, we have used the amplitude  $A = 0.8 \text{ Volt}$  and the frequency  $f_1 = 502 \text{ Hz}$  to assume this subthreshold condition.

We investigated versus both the amplitude  $B$  and the frequency  $f_2$  of the high frequency component whether the system can respond at the low frequency  $f_1$ .

To valid our experiments, we have also performed a numerical analysis of the system behaviour by integrating the normalized system (3) with a fourth order Runge-Kutta algorithm. The integrating time step has been set to  $dt = \frac{100}{N \times f_1}$  where  $N = 2^{20}$  is the total number of sampling points which set the simulation length to  $100/f_1$ , that is one hundred period of the low frequency excitation. Moreover, the initial conditions  $W(\tau = 0) = 0$  and  $V(\tau = 0) = 0$  were systematically used.

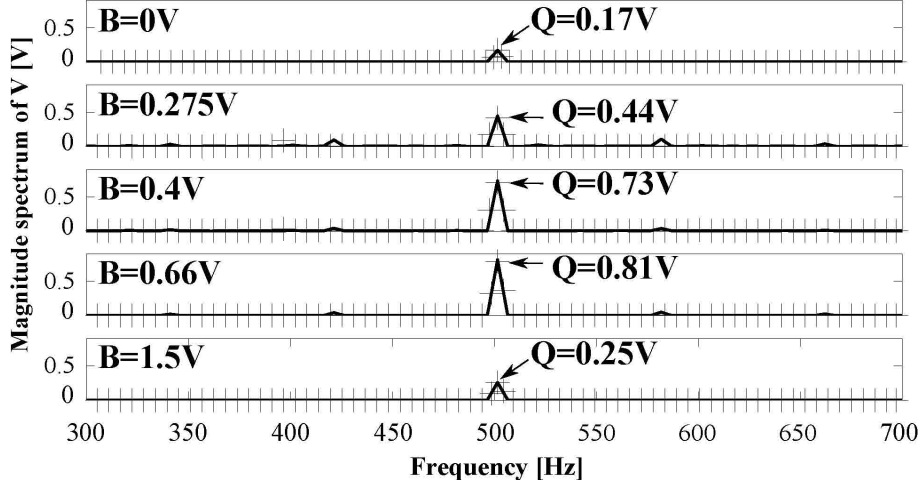


**Fig. 2.** Magnitude spectrum of the voltage  $V$  for different amplitudes  $B$  of the high frequency perturbation. The crosses which correspond to experimental data are compared with the numerical results presented in solid line. The arrows indicate the magnitude  $Q$  obtained numerically at the frequency  $f_1 = 502Hz$ . The parameters are  $a = 2V$ ,  $b = -2.6V$ ,  $E_0 = -1V$ ,  $A = 0.8V$ ,  $f_1 = 502Hz$ ,  $f_2 = 6.1 kHz$ ,  $\gamma = 0.24$  and  $\epsilon = 4.249$ .

### 3 Response of the system at the low frequency $f_1$

To quantize the response of the system at the low frequency  $f_1$ , we have analyzed the behavior of the magnitude spectrum of the voltage  $V$  for different amplitudes  $B$  of the high frequency sinusoidal driving  $f_1$ . The simulation has been plotted in solid line, while the experimental data were superimposed with crosses to enable a direct comparison between numerical results and experiments. All the obtained spectrum are summarized in fig. 2 and they clearly reveal a peak at the low frequency  $f_1$  whose amplitude will be noted  $Q$  in the whole article. To illustrate how the magnitude of this peak behaves, in each spectrum, we have chosen to point this peak at the low frequency  $f_1$  with an arrow and to indicate its value  $Q$  attained numerically.

Both our simulations and our experiments show that the magnitude  $Q$  at the low frequency does not evolve monotonously versus the amplitude  $B$  of the high frequency driving. Especially, it seems to exist an optimal value of  $B$  which maximizes the system's response at the low frequency  $f_1$ . Indeed, as exhibited in fig. 2, the greatest value  $Q = 0.81V$  is obtained in numerical simulation for  $B = 0.66V$  and is almost the same experimentally.

This effect, known as vibrational resonance [1,9], can be highlighted by plotting the spectrum magnitude  $Q$  measured at the low frequency  $f_1$  versus the amplitude  $B$  of the high frequency perturbation. Fig 3 shows the evolution of  $Q$  versus the amplitude  $B$  of the high frequency driving. Despite some discrepancies between experiments and numerical results, a resonant behavior is clearly shown experimentally and confirmed numerically.

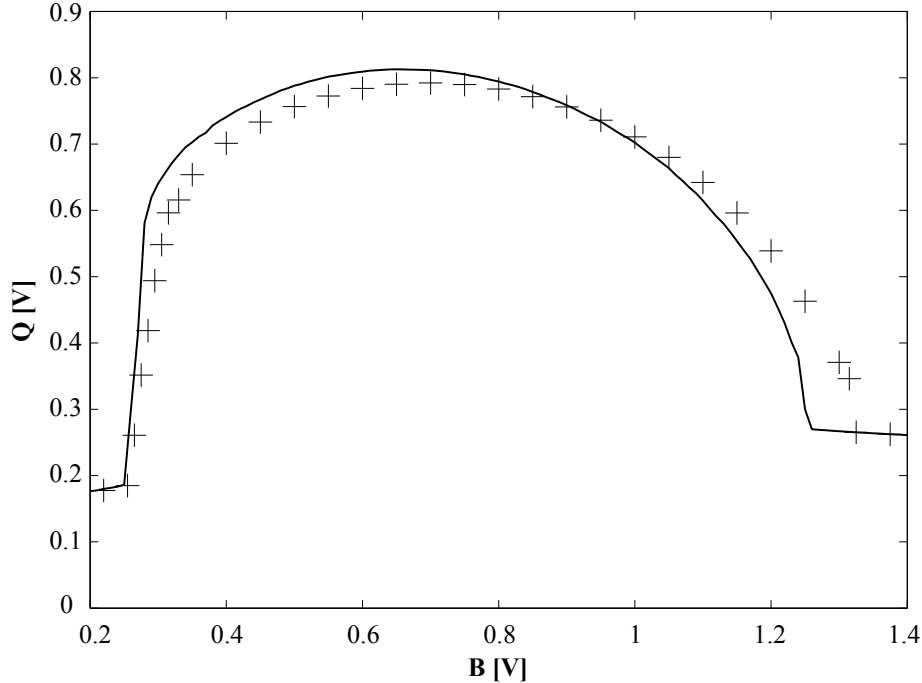


**Fig. 3.** Evolution of the magnitude spectrum  $Q$  estimated at the low frequency  $f_1$  versus the amplitude  $B$  of the high frequency perturbation. The parameters are  $a = 2V$ ,  $b = -2.6V$ ,  $E_0 = -1V$ ,  $A = 0.8V$ ,  $f_1 = 502Hz$ ,  $f_2 = 6.1 kHz$ ,  $\gamma = 0.24$  and  $\epsilon = 4.249$ . The experimental data are plotted with crosses while the simulation results are represented in solid lines.

However, to have an overview of the effect of the high frequency perturbation to the system response, a parametric study of the behaviour of the spectrum magnitude  $Q$  in the amplitude-frequency plane ( $B$ ,  $f_2$ ) is more appropriate than an analysis only restricted to the amplitude  $B$  [10]. We have performed numerically such a 2 dimensional analysis at fig. 4 where the spectrum magnitude  $Q$  is represented in the high frequency range  $[0; 10kHz]$ . For each high frequency  $f_2$ , there exists a value of the perturbation amplitude  $B$  which maximizes the system response at the low frequency  $f_1$ .

As pointed by Yao *etal* in an overdamped bistable oscillator [10], we also observe in the FitzHugh-Nagumo model that there exists two different areas in the amplitude-frequency parameter plane ( $B$ ,  $f_2$ ). Indeed, for high frequencies  $f_2 \gg f_1$ , the maximum of  $Q$  attained by tuning the amplitude  $B$  of the high frequency perturbation is almost constant, while when the two frequencies are of the same order, a greater resonance can be achieved.

Indeed, fig. 5 presents a magnification of fig. 4 in the range of frequencies  $[0; 2.5kHz]$  to better analyze the system response for high frequency  $f_2$  at order of the low frequency  $f_1$ . For this range of frequencies, the system response exhibits peaks located at frequencies multiple and submultiple of the low frequency  $f_1 = 502Hz$  which emerge from the resonant surface shape of

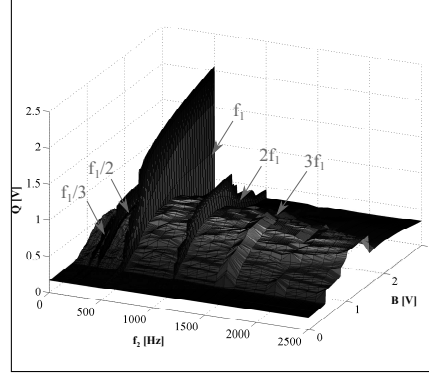
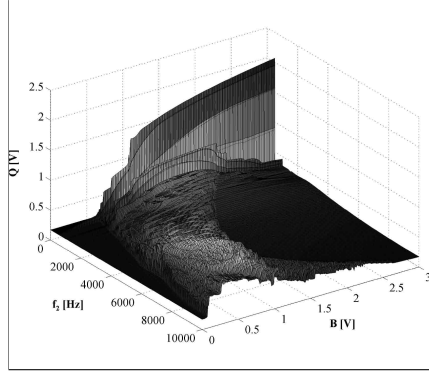


**Fig. 4.** Overview of the magnitude spec-  
trum  $Q$  estimated in numerical simulation  
at the low frequency  $f_1$  in the  $(B, f_2)$  trum  
parametric plane . The parameters are  $f_1$   
in the  $(B, f_2)$  parametric plane . The  
 $a = 2V$ ,  $b = -2.6V$ ,  $E_0 = -1V$ ,  
 $A = 0.8V$ ,  $f_1 = 502Hz$ ,  $f_2 = 6.1 KHz$ ,  
 $E_0 = -1V$ ,  $A = 0.8V$ ,  $f_1 = 502Hz$ ,  
 $\gamma = 0.24$  and  $\epsilon = 4.249$ .

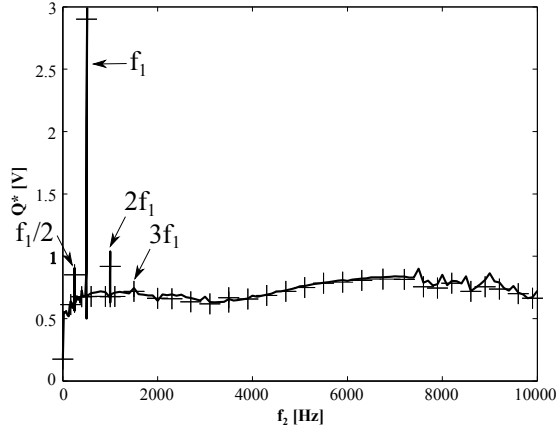
**Fig. 5.** Magnification in the frequency  
range  $[0; 2.5KHz]$  of the magnitude spec-  
trum  $Q$  estimated at the low frequency  
parametric plane . The parameters are  
 $f_1$  in the  $(B, f_2)$  parametric plane . The  
 $a = 2V$ ,  $b = -2.6V$ ,  
 $E_0 = -1V$ ,  $A = 0.8V$ ,  $f_1 = 502Hz$ ,  
 $\gamma = 0.24$  and  $\epsilon = 4.249$ .

Fig. 5. Therefore, an appropriate matching of the high frequency  $f_2$  to the multiple or submultiple of the low frequency  $f_1$  can involve a better resonance. This effect, first highlighted by Yao *etal* [10], is here shown numerically in the FitzHugh-Nagumo system.

To show this effect experimentally, for each value  $f_2$  of the high frequency driving, by varying its amplitude  $B$ , we have determined the maximum value  $Q^*$  reached by the magnitude spectrum  $Q$  at the low frequency  $f_1$ . The evolution of this optimum value is represented in figure 6 versus the high frequency  $f_2$  of the bichromatic excitation. The numerical results in solid line are confirmed by the experimental data plotted by crosses.

A better resonance can be achieved when the frequency  $f_2$  is multiple or submultiple of the low frequency driving  $f_1$ .

Indeed, for  $f_2 = 2f_1$  the simulation provides  $1.05 V$  for the value of  $Q^*$  in fairly good agreement with the value  $0.92 V$  obtained in experiments. Moreover, for  $f_2 = f_1/2$ , the experimental optimum  $Q^*$  for  $Q$  is  $0.85 V$ , that is quite close to the value  $0.9 V$  obtained numerically. For both cases,  $f_2 = 2f_1$  and  $f_2 = f_1/2$ , the optimum attained by  $Q$  exceeds the value  $0.81 V$  provided by vibrational resonance and which corresponds to the continuous background of fig. 6. Lastly, note that the peak achieved for  $f_2 = f_1$  corresponds to the case where  $Q^*$  tends to infinity since increasing  $B$  leads to a monotonous increase of  $Q$ . In experiments, it leads to a saturation of the circuit near  $Q^* = 3V$  instead of infinity.



**Fig. 6.** Evolution of the optimal value of  $Q$  attained versus the high frequency. The parameters are  $a = 2V$ ,  $b = -2.6V$ ,  $E_0 = -1V$ ,  $A = 0.8V$ ,  $f_1 = 502Hz$ ,  $f_2 = 6.1 kHz$ ,  $\gamma = 0.24$  and  $\epsilon = 4.249$ .

## 4 conclusion

This communication was devoted to the analysis of the response of the FitzHugh-Nagumo system submitted to a bichromatic excitation, that is the sum of a low frequency sinusoidal signal perturbed by a high frequency sine wave. An electronic circuit, whose voltages are ruled by the set of FitzHugh-Nagumo equations, has allowed to valid experimentally the behaviours obtained by solving numerically these equations.

Using the magnitude spectrum, we have estimated the system response at the low frequency excitation. Beside the well known classical Vibrational Resonance effect, which occurs when the system response is optimized versus the amplitude of the high frequency perturbation, we have carried out a study in the whole parametric plane defined by both the amplitude and the frequency of the perturbation. In this parametric plane, the system response displays a resonant shape where peaks emerge at multiple and submultiple of the low frequency sinusoidal excitation. This feature reveals that a much better resonance can be obtained by an appropriate matching of the frequencies of the bichromatic excitation. This Frequency Resonance effect which enhances Vibrational Resonance is confirmed experimentally by analyzing the maximum attained by tuning the amplitude of the high frequency perturbation versus its frequency. Lastly, owing to the applications of the FitzHugh-Nagumo in neuroscience and since high frequency perturbation are omnipresent in nature, we trust that our work could be useful in better understanding neural response in perturbed environment.

## Acknowledgements

The research for this work was supported, in part, by the Regional Council of Burgundy.

## References

1. E. Ullner, A. Zaikin, J. Garcia-Ojalvo, R. Bascones and J. Kurths. Vibrational resonance and vibrational propagation in excitable systems, *Phys. Lett. A*, **312**, 348–354, 2003.
2. Y. Chenggui, Y. Liu and Z. Meng. Frequency resonance enhanced vibrational resonance in bistable systems, *Phys. Rev. E*, **83**, 061122, 2011.
3. M. Bordet and S. Morfu. Experimental and numerical study of noise effects in a FitzHugh-Nagumo system driven by a bi-harmonic signal, *Chaos, Solitons and Fractals*, **54**, 82–89, 2013.
4. A.S. Pikovsky and J. Kurths. Coherence resonance in a noise driven excitable system, *Phys. Rev Lett*, **78**, 775–778, 1997.
5. G. Lassere, S. Morfu and P. Marquié. Coherence resonance in a Bonhoeffer Van der Pol circuit, *Electron. Lett.*, **45**, 669–670, 2009.
6. D.R. Chialvo. How we hear what is not there: a neural mechanism for the missing fundamental illusion, *Chaos*, **13**, 1226, 2003.
7. M. Bordet, S. Morfu and P. Marquié. Ghost Stochastic resonance in a FitzHugh-Nagumo circuit, *Electron. Lett.*, **50**, 861–862, 2014.
8. S. Martignoli, F. Gomez and R. Stoop. Pitch sensation involves stochastic resonance, *Scientific Reports*, **3**, 2676, 2013.
9. M. Bordet and S. Morfu. Experimental and numerical enhancement of Vibrational Resonance in a neural circuit, *Electron. Lett.*, **48**, 903, 2012.
10. C. Yao, Y. Liu and M. Zhan. Frequency resonance enhanced vibrational resonance in bistable systems, *Phys. Rev. E*, **83**, 061122, 2011.

# GENERATION OF CHAOTIC ATTRACTOR WITH MULTI-SCROLLS FROM COMPLEX LOGISTIC MAP

K.Bouallegue

Department of Electrical Engineering. Higher Institute of Applied Sciences and  
Technology of Sousse, Tunisia  
kais\_Bouallegue@yahoo.fr

## Abstract

An analytical solution for the well-known quadratic recursion, the logistic map, is presented. Our contribution is to study a logistic map in complex set. In the simulation of the complex logistic map, we observe a plethora of complex dynamic behaviors, which coexist with antagonist form mixed between bifurcation and attractor.

**Keywords:** Logistic map, Chaotic attractor, Bifurcation, Chaos.

## 1 Introduction

The discrete logistic family of maps on the unit interval, given by  $x \rightarrow \lambda(1 - x)$ , has been long studied as a simple but illustrative case of nonlinear iteration.

As with most such smooth families of interval maps, this logistic family exhibits a wide range of behaviors, as the parameter  $\lambda$  rises from 0 to 4. For  $\lambda \leq 1$  ;iterates simply collapse to 0. Above 1, the fixed point at 0 becomes unstable, and a new fixed point arises which attracts the entire open interval (0,1). This behavior persists up through  $\lambda = 3$ , when the period-doubling described by Feigenbaum begins: the fixed point splits into an attractive orbit of period 2, then period 4, and so on, until at last, above the critical parameter 3.57. we arrive to the realm of chaotic behavior, where aperiodic orbits are[1].In this paper, we propose an efficient method to generation multi-scroll chaotic attractor using logistic map.

## 2 Logistic map in Complex set

Being one of the famous equations in physics and biology the logistic map needs no special introduction (a good review of the problem and relevant references can be found in [ 1,2] ).Over the years, the logistic map has long served as perhaps the simplest non-linear discrete time model, and it has been also central in the development and understanding of nonlinear dynamics [4]. In this section, One starts with studying the logistic equation. Generally logistic Map is a one-dimensional map that can produce chaotic behavior [2], [4]

---

*8<sup>th</sup> CHAOS Conference Proceedings, 26-29 May 2015, Henri Poincaré Institute, Paris France*



## 2.1 Logistic map

The logistic map is a paradigmatic model used to illustrate how complex behavior can arise from very simple non-linear dynamical equations [8, 3].

One modifies the logistic equation by a transformation of variable  $x$  by  $z$  one basing itself on the fact  $\mathbb{R} \subset \mathbb{C}$

Let  $Z_1 \in \mathbb{C}$  with

$$Z_1 = x_1 + iy_1$$

The equation of logistics becomes:

$$Z_{n+1} = \lambda Z_n(1 - Z_n)$$

then

$$x_{n+1} + iy_{n+1} = \lambda(x_n + iy_n)(1 - (x_n + iy_n))$$

The equation of logistics becomes a system of equation having the following structure

$$\begin{cases} x_{n+1} = \lambda(x_n) - \lambda(x_n^2 - y_n^2) \\ y_{n+1} = \lambda y_n - 2\lambda x_n y_n \end{cases} \quad (1)$$

The system of equations recurring is equivalent to a function of two variables in  $\mathbb{R}^2$ .

$$\begin{aligned} \mathbb{R}^2 &\longrightarrow \mathbb{R}^2 \\ (F(x, y)) &\longrightarrow \begin{pmatrix} \lambda(x) - \lambda(x^2 - y^2) \\ \lambda y - 2\lambda xy \end{pmatrix} \end{aligned}$$

The system has the form:

$$\begin{pmatrix} x \\ y \end{pmatrix} \longrightarrow \begin{pmatrix} \lambda x(1 - x) - \lambda y^2 \\ \lambda y(1 - 2x) \end{pmatrix}$$

## 2.2 Fixed and equilibrium points

### 2.2.1 Equilibrium points

Let

$$\begin{cases} \lambda(x) - \lambda(x^2 - y^2) = 0 \\ \lambda y - 2\lambda xy = 0 \end{cases} \quad (2)$$

$$\begin{cases} \lambda(x) - \lambda(x^2 - y^2) = 0 \\ y = 0 \end{cases} \quad \text{et} \quad \begin{cases} \lambda(x) - \lambda(x^2 - y^2) = 0 \\ x = \frac{1}{2} \end{cases} \quad (3)$$

there are four equilibrium points  $E_0, E_1, E_2$  et  $E_3$  with,

$E_0(0, 0)$ ,  $E_1(0, 1)$ ,  $E_2(\frac{1}{2}, \frac{1}{\sqrt{2}})$ ,  $E_3(\frac{1}{2}, -\frac{1}{\sqrt{2}})$ , Let us calculate the eigenvalues at the points of stable:

The Jacobian matrix of derivative partial of the equation 3 is given by:

$$J_{E(x^*, y^*)} = \begin{pmatrix} \lambda x^* - 2\lambda x^* & \lambda y^* \\ -2\lambda y^* & \lambda(1 - 2x^*) \end{pmatrix}$$

- For the point of equilibrium  $E_0(0, 0)$ , we find only one eigenvalue and this value is equal to  $\lambda = 1$ .
- For the point of stable  $E_1(0, 1)$ , after computation, we find two eigenvalues and these values are equal to  $\lambda_1 = 1 + i$  et  $\lambda_2 = 1 - i$ .
- For the third case the point of equilibrium  $E_2(\frac{1}{2}, \frac{1}{\sqrt{2}})$  et  $E_3(\frac{1}{2}, -\frac{1}{\sqrt{2}})$  have three eigenvalues and these values are  $\lambda_1 = i\sqrt{2}$  et  $\lambda_2 = -i\sqrt{2}$ .

### 2.2.2 Fixed points

let

$$\begin{cases} \lambda(x) - \lambda(x^2 - y^2) = x \\ \lambda y - 2\lambda xy = y \end{cases} \quad (4)$$

$$\begin{cases} \lambda(x) - \lambda(x^2 - y^2) - x = 0 \\ \lambda y - 2\lambda xy - y = 0 \end{cases} \quad (5)$$

then

$$\begin{cases} \lambda(x) - \lambda(x^2 - y^2) - x = 0 \\ \lambda y - 2\lambda xy - y = 0 \end{cases} \quad (6)$$

The system has four fixed points:

$$E_{(0,0)}, E_1(\frac{\lambda-1}{\lambda}, 0), E_2(\frac{\lambda-1}{2\lambda}, \frac{\sqrt{(1-\lambda)(\lambda+3)}}{2\lambda}), E_2(\frac{\lambda-1}{2\lambda}, -\frac{\sqrt{(1-\lambda)(\lambda+3)}}{2\lambda})$$

## 3 Simulation and results

In this section, we present some numerical simulation of the system 3 for several value of the parameter of  $\lambda$

The following table presents the values of parameter  $\lambda$

$\lambda$	Figure:
4	Fig: 5(a)
0.25	Fig: 5(b)
1.75	Fig: 5(c)
1.95	Fig: 4(c)
1.959	Fig: 3(d)
3.75	Fig: 1(f)

Table 1: Values of implementation for the logistic map

The implementation of this system of equations gave the results illustrated in the figures (5(a), 5(b), 5(c), 4(c),3(d) et 1(f)).

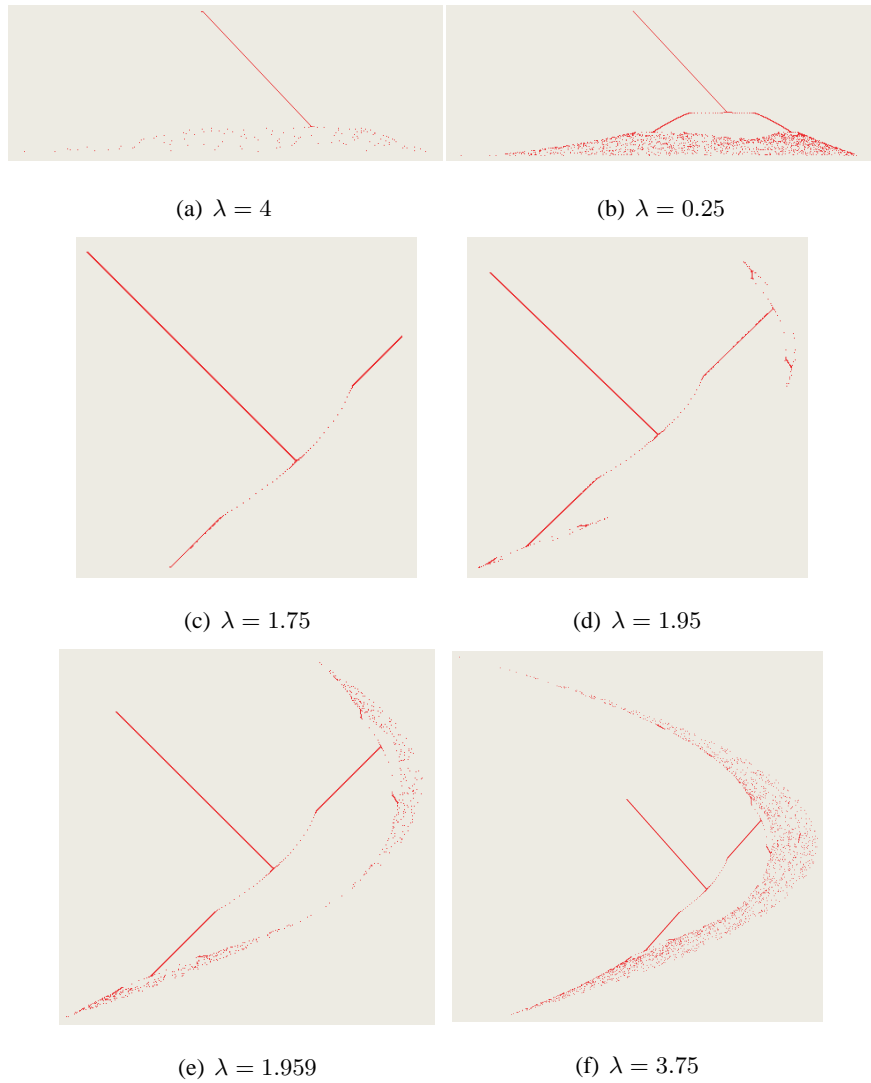


Figure 1: A new logistic map behavior

Figure 5(a) shows the bifurcation form of the new logistic map. This form of behavior changes. When we modify the value of  $\lambda$  from 1 to 4, multi-behavior of bifurcation and attractor appears. if  $\lambda = 3.75$ , a new behavior of antagonist mixed by attractor and bifurcation similar to Hénon attractor.

## 4 Generation of chaotic attractor

### 4.1 Lorenz attractor and logistic map

Several effective techniques have been developed. It is obviously significant to create more complicated chaotic system with multi-scroll or multi-wing attractors, in both theory and engineering application. The celebrated Lorenz system is an approximation of a partial differential equation for a third -order autonomous system.

This system has become one of the paradigms in the research of chaos and is described by:

$$\begin{cases} \dot{x} = \sigma(y - x) \\ \dot{y} = \rho x - y - xz \\ \dot{z} = xy - \beta z \end{cases} \quad (7)$$

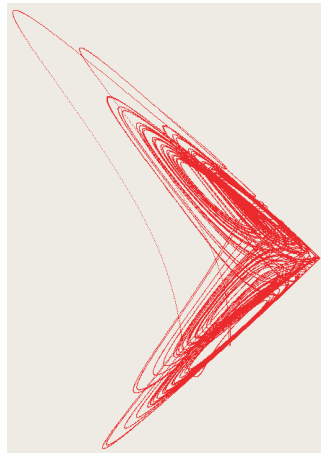
We apply a combination of Julia's process with Lorenz chaotic attractor as follow:

$$(p, q) = P_J(\dot{x}, \dot{y})$$

And then we generate a double states  $u$  and  $v$  using logistic map in complex set.

$$\begin{cases} u = p + \lambda(p(1 - p) - q^2) \\ v = q + \lambda q(1 - 2p) \end{cases} \quad (8)$$

Figure 2 shows results of implementation for only one Julia process.



(a) Behavior of Lorenz chaotic attractor with four scrolls

Figure 2: Behavior of chaotic attractors by logistic map

We apply some different number of combination as follow:

$$(p, q) = P_J \circ P_J \dots P_J(x, y)$$

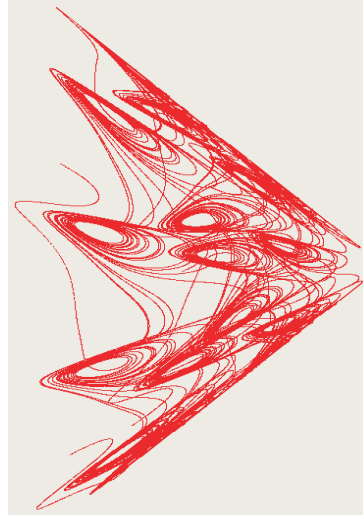
And then we generate a double states  $u$  and  $v$  using logistic map in complex set.

$$\begin{cases} u = p + \lambda(p(1-p) - q^2) \\ v = q + \lambda q(1-2p) \end{cases} \quad (9)$$

Figure 5 shows results of implementation with different number of Julia processes in cascades.



(a)  $P_J o P_J (n = 2)$



(b)  $P_J o P_J o P_J (n = 3)$



(c)  $P_J o P_J o P_J o P_J (n = 4)$



(d)  $(n = 5)$

Figure 3: Behavior of chaotic attractors with multi scrolls

## 4.2 Chua attractor and logistic map

Chua's circuits, which were introduced by Leon Ong Chua in 1983, are simple electric circuits operating in the mode of chaotic oscillations[7].

Different dynamic system were deduced from Chua circuit such as:

$$\begin{cases} \dot{x}_1 = x_2 \\ \dot{x}_2 = x_3 \\ \dot{x}_3 = a(-x_1 - x_2 - x_3 + f(x_1)) \end{cases} \quad (10)$$

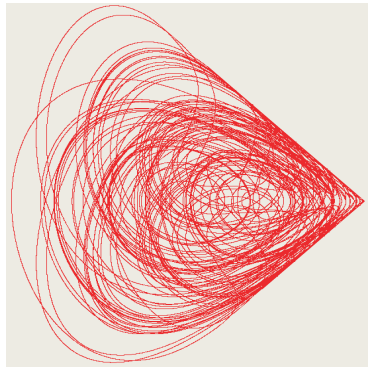
where  $\dot{x}, \dot{y}$  and  $\dot{z}$  are the first time derivatives,  $a$  is a real parameter, and  $f(x_1)$  is a saturated function defined below:

$$f(x) = \begin{cases} k, & \text{if } x > 1 \\ kx, & \text{if } |x| < 1 \\ -k, & \text{if } x < -1 \end{cases} \quad (11)$$

We apply a combination of Julia's process with Chua chaotic attractor as follows:

$$(p, q) = P_J(\dot{x}, \dot{y})$$

$$\begin{cases} u = p + \lambda(p(1-p) - q^2) \\ v = q + \lambda q(1-2p) \end{cases} \quad (12)$$



(a)  $P_J$



(b)  $P_J o P_J$



(c)  $P_J o P_J o P_J$

Figure 4: Behavior of Chua chaotic attractor with multi scrolls

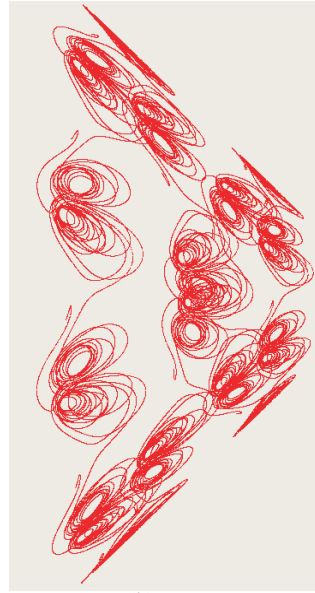
### 4.3 Combination between Lorenz attractor and Chua attractor

We apply a combination of Julia's process with subtract states between Chua chaotic attractor from Lorenz chaotic attractor as follow:

$$\begin{aligned}(p, q) &= P_J(\dot{x}_c - \dot{x}_l, \dot{y}_c - \dot{y}_l) \\(p_3, q_3) &= P_J \circ P_J \circ P_J P_J(p, q) \\ \begin{cases} u = p_3 + \lambda(p_3(1 - p_3) - q_3^2) \\ v = q_3 + \lambda q_3(1 - 2p_3) \end{cases} & \quad (13)\end{aligned}$$



(a)  $x_c - x_l, y_c - y_l$



(b)  $x_c - z_l, y_c - y_l$



(c)  $x_c - z_l, y_c - x_l$

Figure 5: Behavior of chaotic attractors for different states

## 5 Concluding remarks

In this paper we have mainly studied the logistic map in a complex set. As we have shown the new system is able to generate chaos in wide range of parameter  $\lambda$  and even we have observed an interesting phenomena mixed of the behavior attractor and behavior bifurcation. The effectiveness of the proposed schemes is demonstrated through computer simulation. Therefore, the proposed novel logistic maps enrich the nonlinear dynamical system through the extra degree of freedom which can be used for the accurate study and modeling of many applications in various fields as in bioinformatics and nanotechnology.

## References

- [1] David Steinsaltz (2001) Random logistic maps and Lyapunov exponents *Indag. Mathem., N.S.*, **12**,(4), 557 – 584
- [2] R.C. Hilborn,(1994) Chaos and Nonlinear Dynamics,*Oxford Univ. Press,Oxford.*
- [3] R.M. May,(1976) *Nature* 261, 459.
- [4] P. Collet, J.P. Eckmann,(1980) Iterated Maps on the Interval as Dynamical Systems, Birkhäuser, Boston, .
- [5] Erik A. Levinsohn, Steve A. Mendoza, Enrique Peacock-López (2012) Switching induced complex dynamics in an extended logistic map *Chaos, Solitons & Fractals* **45**,426 – 432
- [6] Crenshaw, B.,III, and Jones, W.B.,Jr (2003) The future of clinical cancer management: one tumor, one chip. *Bioinformatics*, doi:10.1093/bioinformatics/btn000.
- [7] Chua, L. O., Komuro, M. & Matsumoto, T. [1986]”The double scroll family,”*IEEE Trans. Circuits Syst* **33**, pp. 1072–1118.
- [8] Zenonas.Navickas,Minvydas.Ragulskis,Alfonasas.Vainoras,Rasa.Smidtaite(2012)The explosive divergence in iterative maps of matrices *Commun Nonlinear Sci Numer Simulat***17** 4430 – 4438
- [9] Gidea M, Gidea C, Byrd W.(2011) Deterministic models for simulating electrocardiographic signals. *Commun Nonlinear Sci Numer Simulat* ;**16**:3871 – 80.

- [10] Wu X, Guan Z-H.(2007) A novel digital watermark algorithm based on chaotic maps. *Phys Lett A* ;**365**(5 – 6) : 403 – 6.
- [11] Rogers A, Keating JG, Shorten R, Heffernan DM.(2002) Chaotic maps and pattern recognition-the XOR problem. *Chaos Soliton Fract* ;**14**:57 – 70.
- [12] Fridrich J.(1998) Symmetric ciphers based on two-dimensional chaotic maps. *Int J Bifurcat Chaos* ;**8,6**:1259 – 84.
- [13] Elhadj Z, Sprott JC.(2008) A two-dimensional discrete mapping with C1 multifold chaotic attractors. *Electron J Theor Phys* ; **5,17**:107 – 20.

# Unveiling complexity of church bells dynamics using experimentally validated hybrid dynamical model

Piotr Brzeski<sup>1</sup>, Tomasz Kapitaniak<sup>1</sup>, and Przemyslaw Perlikowski<sup>1,2</sup>

<sup>1</sup> Division of Dynamics, Technical University of Lodz, Stefanowskiego 1/15, 90-924 Lodz, Poland

(E-mail: [piotr.brzeski@p.lodz.pl](mailto:piotr.brzeski@p.lodz.pl))

<sup>2</sup> Department of Civil & Environmental Engineering, National University of Singapore, 1 Engineering Drive 2, Singapore 117576, Singapore

(E-mail: [przemyslaw.perlikowski@p.lodz.pl](mailto:przemyslaw.perlikowski@p.lodz.pl))

**Abstract.** We investigate the dynamics of the yoke-bell-clapper impacting system using a novel hybrid dynamical model, which is verified experimentally by comparing the results of numerical simulations with experimental data obtained from the biggest bell in the Cathedral Basilica of St Stanislaus Kostka, Lodz, Poland. Having proved that the model is a reliable predictive tool we present a plethora of different dynamical behaviours that can be observed in the considered system. We highlight the solutions that can be considered as a proper working regimes of the instrument and describe how to obtain them. Detailed bifurcation analysis allow us to present how the design of the yoke and propulsion mechanism influence the response of the system. Presented results prove the feasibility of the developed model and demonstrate the importance of nonlinear analysis in practical engineering applications.

**Keywords:** Bells dynamics, Bifurcation analysis, Impacting system, Hybrid system, Computer simulations, Experimental verification.

## 1 Introduction

Bells are musical instruments that are closely connected with European cultural heritage. Although the design of a bell, its clapper and a belfry has been developed for centuries, mathematical modeling of their behaviour have been encountered recently. It is surprising from an engineering point of view because bells and their supports are structures that are exposed to severe loading conditions during ringing. To ensure that they will work reliably for ages, we have to consider many factors and one of the most important is to ensure safe and effective operation. Moreover, the dynamics a yoke-bell-clapper system is extremely complex and difficult to analyze due to its nonlinear characteristic, repetitive impacts and complicated excitation.

The first attempt to describe bell's behaviour using equation of motion was made by Veltmann in 19th century [1,2]. His work was stimulated by the

---

*8<sup>th</sup> CHAOS Conference Proceedings, 26-29 May 2015, Henri Poincaré Institute, Paris France*

© 2015 ISAST



failure of the famous Emperor's bell in the Cologne Cathedral when the clapper remained always on the middle axis of the bell instead of striking it. Veltmann explained the reason of this phenomena using simple model developed basing on the equations of a double physical pendulum. Heyman and Threlfrall [3] use similar model to estimate inertia forces induced by a swinging bell. The knowledge of loads induced by ringing bells depends on the mounting layout and is crucial during the design and restoration processes of belfries. In Europe one can distinguish three different types of swinging bells: Central European, English and Spanish. In the first of them, bells tilt on their axis and maximum amplitude of oscillation is usually below 90 degrees. In the English system bells perform nearly a complete rotation (the bell stops close to upper position); while in the Spanish system bells rotate continuously in the same direction.

Muller [4] and Steiner [5] analyze the dynamic interactions between bells and bell towers and describe the dynamic forces appearing in bells mounted in Central European manner. There are also similar studies concerning English system [6,7] as well as Spanish system [8,9]. Ivorra et. al. [10,11] show how mounting layout affects the dynamic forces induced by bells. Authors prove that in the Spanish system forces transmitted to the supporting structure are significantly lower than in English and Central European. Nevertheless, studies described in [12,13] prove that often minor modification in support's design can significantly decrease the probability of damage of the bell tower.

Klemenc et. al. contributed with a series of papers [14,15] devoted to the analysis of the clapper-to-bell impacts. Presented results prove that full-scale finite-element model is able to reproduce the effect of collisions but requires long computational times and complex, detailed models. Therefore, it would be difficult to use such models to analyze the dynamics of bells. Because of that, recently we observe the tendency to use hybrid dynamical models which are much simpler and give accurate results with less modeling and computational effort. In [16] authors propose lumped parameter model of the bells mounted in Central European system and prove that with the model we are able to predict impact acceleration and bell's period of motion.

The paper is organized as follows. In Section 2 we describe the hybrid dynamical model of the church bell and validate it by comparing the results of numerical simulations with data obtained experimentally. In Section 3 we characterize the 7 most common working regimes and in Section 4 investigate how they can be obtained. Finally, in Section 5 the conclusions are drawn.

## 2 Model of the system

The model that is presented in this paper is build up based on the analogy between freely swinging bell and the motion of the equivalent double physical pendulum. The first pendulum has fixed axis of rotation and models the yoke and the bell that is mounted on it. The clapper is imitated by the second pendulum attached to the first one. Proposed model involves eight physical parameters. The photo of the bell that has been measured to obtain the parameters values is presented in Fig.1 (a). In Figs.1 (b,c) we show schematic model of the bell indicating the position of the rotation axes of the bell the

clapper and presenting parameters involved in the model. For simplicity, henceforth, we use term “bell” with respect to the combination of the bell and its yoke which we treat as one solid element.

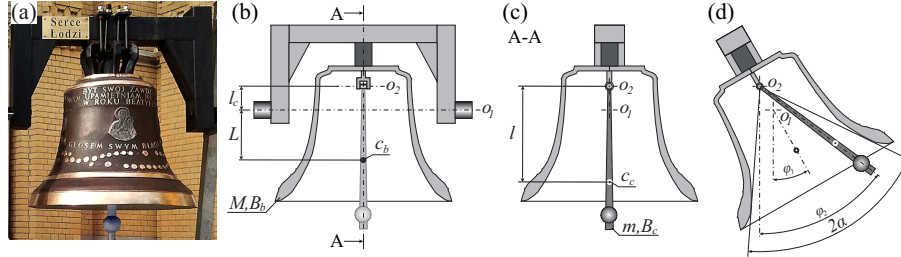


**Fig. 1.** “The Heart of Lodz” the biggest bell in the Cathedral Basilica of St Stanislaus Kostka (a) and its schematic model (b,c,d) along with physical and geometrical quantities involved in the mathematical model of the system.

Parameter  $L$  describes the distance between the rotation axis of the bell and its center of gravity (point  $C_b$ ),  $l$  is the distance between the rotation axis of the clapper and its center of gravity (point  $C_c$ ). The distance between the bell’s and the clapper’s axes of rotation is given by parameter  $l_c$ . Mass of the bell is described by parameter  $M$ , while parameter  $B_b$  characterizes the bell’s moment of inertia referred to its axis of rotation. Similarly, parameter  $m$  describes the mass of the clapper and  $B_c$  stands for the clapper’s moment of inertia referred to its axis of rotation.

Considered model has two degrees of freedom. In Fig. 1 (d) we present two generalized coordinates that we use to describe the state of the system: the angle between the bell’s axis and the downward vertical is given by  $\varphi_1$  and the angle between the clapper’s axis and downward vertical by  $\varphi_2$ . Parameter  $\alpha$  (see 1 (d)) is used to describe the clapper to the bell impact condition which is as follows:

$$|\varphi_1 - \varphi_2| = \alpha \quad (1)$$

We use Lagrange equations of the second type and derive two coupled second order ODEs that describe the motion of the considered system (full derivation can be found in our previous publication [17]):

$$(B_b + ml_c^2) \ddot{\varphi}_1 + ml_cl\ddot{\varphi}_2 \cos(\varphi_2 - \varphi_1) - ml_cl\dot{\varphi}_2^2 \sin(\varphi_2 - \varphi_1) \quad (2)$$

$$+ (ML + ml_c) g \sin \varphi_1 + D_b \dot{\varphi}_1 - D_c (\dot{\varphi}_2 - \dot{\varphi}_1) = M_t(\varphi_1),$$

$$B_c \ddot{\varphi}_2 + ml_cl\dot{\varphi}_1 \cos(\varphi_2 - \varphi_1) + ml_cl\dot{\varphi}_1^2 \sin(\varphi_2 - \varphi_1) \quad (3)$$

$$+ mgl \sin \varphi_2 + D_c (\dot{\varphi}_2 - \dot{\varphi}_1) = 0.$$

where  $g$  stands for gravity and  $M_t(\varphi_1)$  describes the effects of the linear motor propulsion. The motor is active - and excites the bell - when its deflec-

tion from vertical position is smaller than  $\pi/15$  [rad] ( $12^\circ$ ). The generalized momentum generated by the motor  $M_t(\varphi_1)$  is given by the piecewise formula:

$$M_t(\varphi_1) = \begin{cases} T \operatorname{sgn}(\dot{\varphi}_1) \cos(7.5\varphi_1), & \text{if } |\varphi_1| \leq \frac{\pi}{15} \\ 0, & \text{if } |\varphi_1| > \frac{\pi}{15} \end{cases} \quad (4)$$

where  $T$  is the maximum achieved torque. Although the above expression is not an accurate description of the effects generated by the linear motor, in [17] we prove that it is able to reproduce the characteristics of the modern bells' propulsions.

There are eleven parameters involved in the mathematical model presented above. The parameters have the following values:  $M = 2633$  [kg],  $m = 57.4$  [kg],  $B_b = 1375$  [kgm<sup>2</sup>],  $B_c = 45.15$  [kgm<sup>2</sup>],  $L = 0.236$  [m],  $l = 0.739$  [m],  $l_c = -0.1$  [m] and  $\alpha = 30.65^\circ = 0.5349$  [rad],  $D_c = 4.539$  [Nm s],  $D_b = 26.68$  [Nm s],  $T = 229.6$  [Nm]. As aforementioned, all parameters values have been evaluated specifically for the purpose. For integration of the model described above we use the fourth-order Runge–Kutta method.

When the condition 1 is fulfilled we stop the integration process. Then, instead of analyzing the collision course, we restart simulation updating the initial conditions of equations 2 and 3 by switching the bell's and the clapper's angular velocities from the values before the impact to the ones after the impact. The angular velocities after the impact are obtained taking into account the energy dissipation and the conservation of the system's angular momentum that are expressed by the following formulas:

$$\frac{1}{2}B_c(\dot{\varphi}_{2,AI} - \dot{\varphi}_{1,AI})^2 = k\frac{1}{2}B_c(\dot{\varphi}_{2,BI} - \dot{\varphi}_{1,BI})^2, \quad (5)$$

$$\begin{aligned} & [B_b + ml_c^2 + ml_c l \cos(\varphi_2 - \varphi_1)] \dot{\varphi}_{1,BI} + [B_c + ml_c l \cos(\varphi_2 - \varphi_1)] \dot{\varphi}_{2,BI} = \\ & [B_b + ml_c^2 + ml_c l \cos(\varphi_2 - \varphi_1)] \dot{\varphi}_{1,AI} + [B_c + ml_c l \cos(\varphi_2 - \varphi_1)] \dot{\varphi}_{2,AI} \end{aligned} \quad (6)$$

where index *AI* stands for “after impact”, index *BI* for “before impact” and parameter  $k$  is the coefficient of energy restitution. In our simulations we assume  $k = 0.05$  referring to a series of experiments performed by Rupp et al. [18]. In our previous investigation [17] we have analyzed influence of  $k$  on the response of the system and we have proved that system's dynamics barely changes for small alterations of parameter  $k$  ( $\pm 20\%$ ). Hence, we claim that there is no need to further adjust the value of  $k$  for the considered bell. ODEs 2 and 3 together with the discrete model of impact create a hybrid dynamical system that can be used to simulate the behaviour of church bells.

## 2.1 Validation of the model

In this Section we investigate the full model and validate it focusing on normal ringing conditions. Our study is based on the bell in the Cathedral Basilica of

St Stanislaus Kostka and we check the reliability of the model by comparing the results of numerical simulations with experimentally obtained time traces of “*The Heart of Lodz*”.

We have launched the linear motor propulsion and after a start-up procedure, when the amplitude of the bell’s motion stabilized, we have begun recording with high-speed camera (Basler piA640-210gm). We have used black-and-white stickers to mark the position of the bell, the clapper and indicate reference length. We have used Kinovea software to create - basing on the recordings - the data-sheets with markers’ abscissa and ordinate depending on time and processed the data in Mathematica software.

In Fig. 2 we compare the results of numerical simulations and time traces obtained from two separate recordings. In subplots (a,b) we present data collected from the first recording and in subplots (c,d) from the second one. Red lines in Fig. 2 represent periodic attractor obtained numerically and black dots correspond to experimental results. In subplots (a) and (c) we show time traces of the bell while subplots (b) and (d) are devoted to the clapper’s behavior. Comparing the trajectories of the bell one can say that numerical results show remarkable agreement with the experiment. Simultaneously, time traces of the clapper do not show such a convergence as the clapper of the examined bell performed non-periodic motion. Divergence form numerically obtained periodic attractor is mainly visible around the moments of impact.

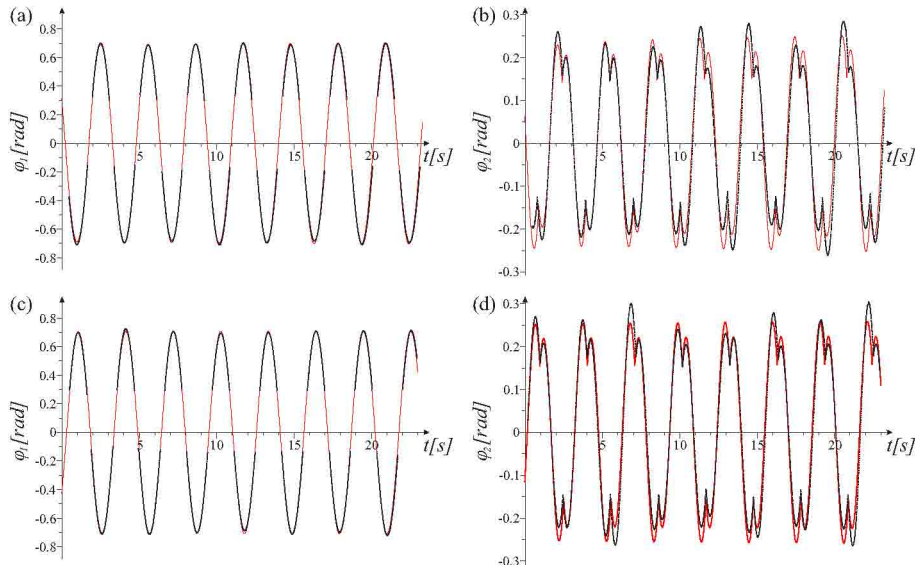


**Fig. 2.** Comparison between time traces of the bell (a,c) and the clapper (b,c) obtained numerically (red lines) and experimentally (black dots). Subplots (a,b) correspond to the data obtained from the first recording and (c,d) from the second one.

Analyzing Fig. 2 one can say that hybrid model introduced in this paper is able to simulate the bell’s behavior with excellent accuracy and precisely

determine crucial features of the clapper's motion such as: the period of motion, average amplitude of motion and predict moments of the clapper to the bell collisions. Still, slight divergence between the lines is visible around the moments of impacts. It is caused by the oscillations of the bell's shell which are not included in the mathematical model of the system. In [17] we describe this phenomenon in detail and prove that it do not compromise the reliability and practical significance of the considered model.

## 2.2 Influencing parameters

Most of the parameters involved in the model are self dependent. Moreover, we have to remember that we investigate a musical instrument, hence we cannot change some of its features that could affect the sound it generates. The two features that we can safely modify in real applications are the driving motor and the yoke of the bell. Therefore, we analyze how such changes influence the system's dynamics. As a reference, we use values of parameters characteristic for “*The Heart of Lodz*” and alter them to simulate modifications in the propulsion or mounting layout. We assume the linear motor driving that is described by piecewise function  $M_t(\varphi_1)$  4 and modify the output of the motor by changing the maximum generated torque  $T$  which we use as the first controlling parameter. To describe the modifications of the yoke we introduce the second parameter  $l_r$  whose meaning is described in Fig. 3.

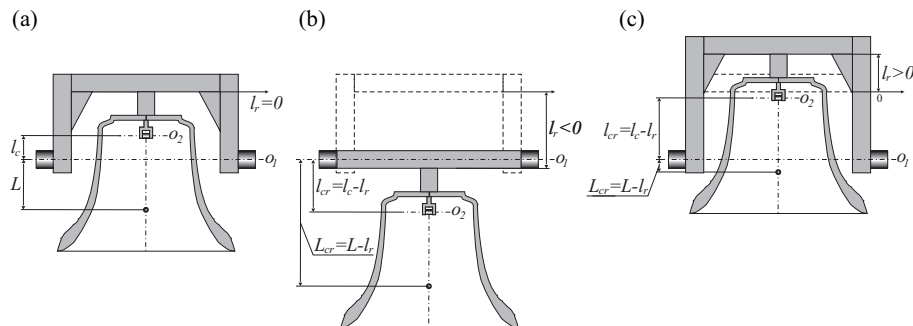


**Fig. 3.** Description of parameter  $l_r$ : (a) reference yoke design  $l_r = 0$ , (b)  $l_r < 0$ , (c)  $l_r > 0$ .

We take “*The Heart of Lodz*” as a reference yoke for which  $l_r = 0$ . If the bell's center of gravity is lowered, then  $l_r < 0$  and as the value of  $l_r$  we take the distance by which the bell's center of gravity is shifted with respect to the reference yoke. Similarly, if we elevate the bell's center of gravity, we assume  $l_r > 0$  and take its displacement as the value of  $l_r$ . As a maximum considered value of  $l_r$  we take  $0.235 [m]$  because for  $l_r = 0.236 [m]$  rotation axis of the bell goes through its center of mass.

It should be stressed out that each changes of  $l_r$  value affect other parameters of the model. So, when the value of  $l_r$  is changed the three different parameters should be swapped:  $L$  has to be replaced by  $L_r$ ,  $l_c$  by  $l_{cr}$ , and

finally  $B_b$  by  $B_{br}$ . New parameters  $L_r$ ,  $l_{cr}$  and  $B_{br}$  are given by the following formulas:

$$L_r = L - l_r$$

$$l_{cr} = l_c - l_r \quad (7)$$

$$B_{br} = (B_b - ML^2) + ML_r^2$$

### 3 Most common bells' working regimes

In this section we present and describe periodic attractors that can be considered as a proper working regimes and have practical applications. These regimes are often called ringing schemes and can be classified in groups that have common characteristics such as especially: number of collisions during one period of motion, course of collisions and time between them. In Fig. 4 we present 6 most common working regimes by showing phase portraits of the bell and the clapper (blue lines) and indicating the effects of collisions (red lines). Subplots of Fig. 4 were obtained for different values of parameters  $T$  and  $l_r$ .

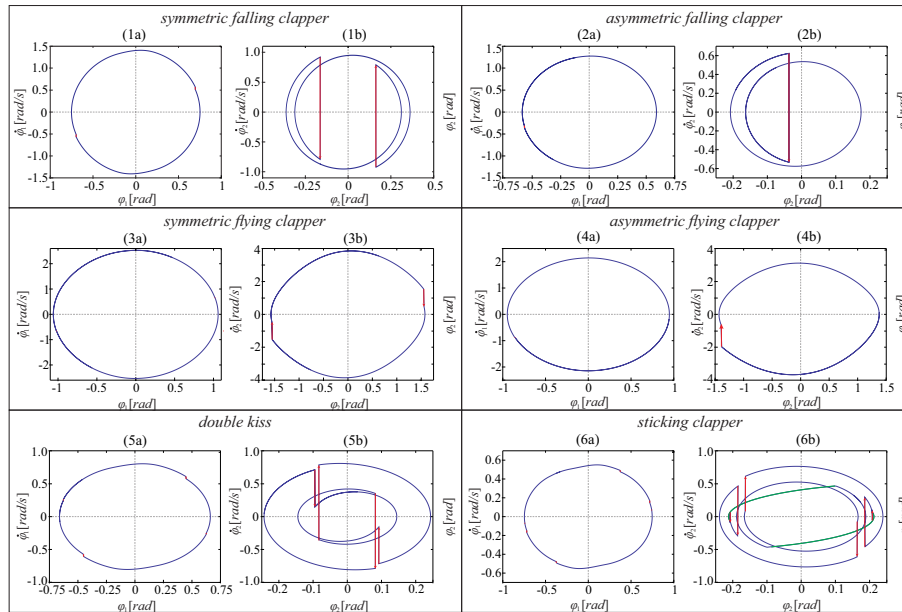


**Fig. 4.** Presentation of the most common working schemes of church bells. Subplots (a) and (b) present phase portraits of the bell and the clapper respectively.

We say that the bell works in a “falling clapper” manner if the collisions between the bell and the clapper occur when they perform an anti-phase motion (see Figs. 4 (1), (2) ). This type of behavior is common for bells that are

mounted in the European manner. In the "falling clapper" ringing scheme the amplitude of the clapper's motion is smaller than the bell's; and the clapper's velocity sign changes when collision occurs. We can distinguish a symmetric type of "falling clapper" with 2 collisions per one period of motion (Figs. 4 (1a-b) obtained for  $T = 350 [Nm]$  and  $l_r = 0.05 [m]$ ) and its asymmetric version with 1 impact per period (Figs. 4 (1a-b) obtained for  $T = 150 [Nm]$  and  $l_r = -0.03 [m]$ ). These ringing schemes differ mainly in the time intervals between the successive impacts.

The second characteristic working regime is called "flying clapper". In this regime collisions occur when the bell and the clapper perform in-phase motion. The amplitude of the clapper's motion is larger than the bell's; and the clapper's velocity sign remains the same after the collisions. The collisions have more gentle course than in the "falling clapper" manner, hence sometimes it may be difficult to achieve nice resounding of the bell. In Figs. 4 (3) and (4) we present two types of "flying clapper" behavior: symmetric attractor with 2 impacts per period obtained for  $T = 450 [Nm]$ ,  $l_r = -0.91 [m]$  and asymmetric one with only 1 impact per period that we receive for  $T = 325 [Nm]$  and  $l_r = -1.21 [m]$ .

Bells mounted in English manner usually works in the "sticking clapper" regime in which the clapper and the bell remain in contact for a certain amount of time. In the considered system prior the sliding mode we observe a number of successive impacts (usually 3) that have a "falling clapper" course. In Fig. 4 (6) we show phase portraits of the bell (6a) and the clapper (6b) working in the "sticking clapper" manner obtained for  $T = 125 [Nm]$  and  $l_r = 0.2 [m]$ . The energy amount that is transferred between the bell and the clapper decreases with each subsequent collision. Hence, the sound effects caused by each hit are different and not all collisions may be noticed by the listener.

Rarely we can observe the so-called "double kiss" working regime in which we observe 4 impacts per one period of motion (see Fig. 4 (5) obtained for  $T = 175 [Nm]$  and  $l_r = 0.16 [m]$ ). During one period the clapper hits each side of the bell's shell twice. The first collision on each side is in the "falling clapper" manner while the second impact has "flying clapper" course. This behavior is especially attractive for the listeners but it is difficult to achieve.

Apart from the described above we can also observe stable periodic attractors with no collisions, but then no sound is produced and the bell can not work as a musical instrument. Unfortunately, no impacting attractors occur in wide range of  $T$  and  $l_r$  values. Moreover, we can distinguish other periodic attractors that can be successfully employed such as asymmetric "flying clapper" behavior with doubled period and 4 impacts per period that can be easily taken as a typical "flying clapper". Similarly, a quasi-periodic attractor with almost equal time intervals between the subsequent impacts can sound almost like a periodic ringing scheme. In the next Section we analyze how the most common working schemes can be achieved by proper designing the propulsion mechanism and the yoke of the bell.

## 4 Influence of the yoke design and forcing amplitude on the system's dynamics

The yoke's design - described by parameter  $l_r$  - and the amplitude of forcing - parameter  $T$  - define the working regime of the bell. In this section we analyze how these parameters influence the response of the system. In Fig. 5 we show the result of series of numerical simulations obtained using 154 different sets of parameters values from the following ranges:  $l_r \in \langle -1.3, 0.23 \rangle [m]$  and  $T \in \langle 100, 625 \rangle [Nm]$ . For each set of parameters we start the simulation from zero initial conditions ( $\varphi_1 = 0, \varphi_2 = 0, \dot{\varphi}_1 = 0, \dot{\varphi}_2 = 0$ ) and mark on the plot which ringing scheme we obtain. We concern only the solutions that basins of attraction contain zero initial conditions ( $\varphi_1 = 0, \varphi_2 = 0, \dot{\varphi}_1 = 0, \dot{\varphi}_2 = 0$ ). Such approach is practically justified because in most cases the bell and the clapper start their motion from hanging down position with zero velocities.

We consider 7 most characteristic types of the bells behavior that are described in detail in the previous Section.

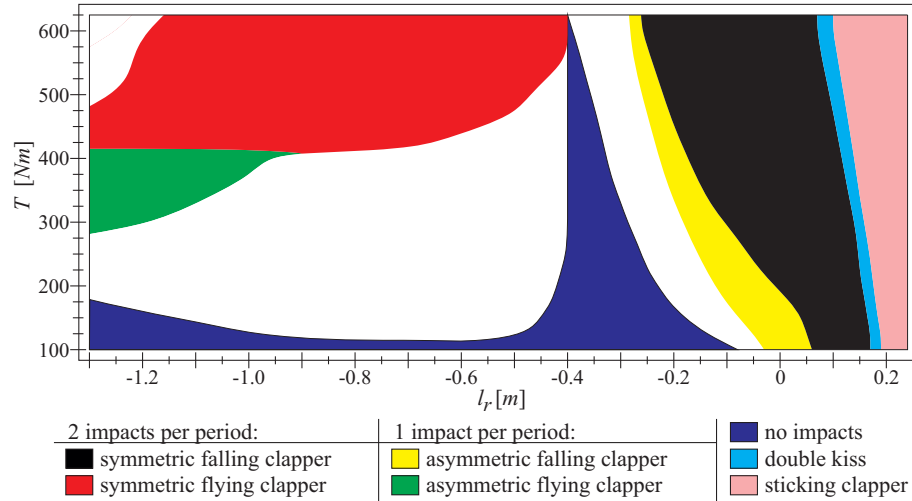


**Fig. 5.** Two parameter ringing schemes diagram showing the behavior of the system for different values of  $l_r$  and  $T$ .

Analyzing Fig. 5 we see that the biggest areas correspond to the three most common ringing schemes: symmetric “falling clapper” (black) and “flying clapper” (red) and “sticking clapper” (pink) that is typical for the bells mounted in the English manner. Thanks to that, these behaviors are relatively easy to achieve and remain even after long period of time when values of some parameters can change a bit (for example maximum torque generated by the linear motor). We see that, in general, the design of the yoke determines how the bell will operate. For  $l_r < -0.4 [m]$  we can observe “flying clapper” with 2 (red) or 1 (green) impacts per period but these ringing schemes can be achieved only when  $T$  is bigger than some threshold value which decreases with

the decrease of  $l_r$ . If  $T$  is not sufficient we will not observe any impacts (blue) or the system will reach different attractor (white) - periodic or non-periodic one. For  $l_r \in (-0.4, -0.284)$  [m] we cannot obtain any of the analyzed ringing schemes despite the forcing amplitude. Hence, when the yoke is designed improperly it may be impossible to force the system to ensure proper operation. For  $l_r > -0.284$  [m] the system can work in the following manner: “falling clapper” with 1 (yellow) or 2 (black) impacts per period, “double kiss” (light blue) or “sticking clapper” (pink). Each of these ringing schemes can be achieved despite the value of  $T$  but the yoke should be designed for the purpose. Hence, for these working regimes there is no need to use very powerful driving motors and the system can work more efficiently. In our previous publication [19] we consider transitions between different dynamical states of the yoke-bell-clapper system and analyse the time that is needed to reach presumed solution.

## 5 Conclusions

In this paper we investigate a plethora of different dynamical behaviors encountered during the analysis of the hybrid dynamical model of the church bell. The model is developed basing on the bell in the Cathedral Basilica of Stanislaus Kosta, Lodz, Poland. Its parameters values are determined during the series of measurements and experiments involving the bell [17]. Finally, we validate the model by comparing the results of numerical simulations with experimental data and prove that it provides all crucial information about the system’s dynamics which is beneficial for bell-founders, bell-hangers and engineers working on bells or bell towers.

In the next part of the paper we focus on solutions that can be considered as a proper working regimes of the instrument. We present and characterize the 6 most common behaviours and present a method that can be used to determine the conditions under which given type of behavior can be achieved. We use the amplitude of the forcing  $T$  and the yoke design (described by the parameter  $l_r$ ) as the influencing parameters and develop two parameters ringing scheme diagrams. Such plots provide full information on how the geometry of the yoke and maximum output of the driving motor influence the dynamics of the system.

Ringing scheme charts can be calculated for any bell and used to design its yoke and propulsion. Presented tools can help to improve working conditions of existing bells as well as during the design of mounting layouts for new instruments. Thus, using the numerical analysis of the systems dynamics we can ensure that the bell will work properly and reliably for ages and regardless of small changes of parameters.

## Acknowledgment

This work is funded by the National Science Center Poland based on the decision number DEC-2013/09/N/ST8/04343.

We would especially like to thank the Parson of Cathedral Basilica of St Stanislaus Kostka Prelate Ireneusz Kulesza for his support and unlimited access to the bell. We have been able to measure the bell's template thanks to the bell's founder Mr Zbigniew L. Felczyński. The data on the clapper, the yoke and the motor have been obtained from Mr. Paweł Szydłak.

## References

1. W. Veltmann. Uerber die bewugun einer glocke. *Dinglers Polytechnisches Journal*, 220:481–494, 1876.
2. W. Veltmann. Die koelner kaiserglocke. enthullungen uber die art und weise wie der koelner dom zu einer mirathenen glocke gekommen ist. *Hauptmann, Bonn*, 1880.
3. BD. Threlfall J. Heyman. Inertia forces due to bell-ringing. *International Journal of Mechanical Sciences*, 18:161–164, 1976.
4. FP. Muller. Dynamische und statische gesichtspunkte beim bau von glockenturmen. *Karlssruhe: Badenia Verlag GmbH*, pages 201–212, 1986.
5. J. Steiner. Neukonstruktion und sanierung von glockenturmen nach statischen und dynamischen gesichtspunkten. *Karlssruhe: Badenia Verlag GmbH*, pages 213–237, 1986.
6. A. Selby J. Wilson. Durhamm cathedral tower vibrations during bell-ringing. In *Proceedings of the conference engineering a cathedral.*, pages 77–100. London: Thomas Telford, 1993.
7. A. Selby J. Wilson. Dynamic behaviour of masonry church bell towers. In *Proceedings of the CCMS symposium*, pages 189–199. New York: Chicago ASCE, 1997.
8. S. Ivorra and J. R. Cervera. Analysis of the dynamic actions when bells are swinging on the bell-tower of bonrepos i mirambell church (valencia, spain). *IProc. of the 3rd international seminar of historical constructions*, pages 413–19, 2001.
9. S. Ivorra and F. J. Pallares. Dynamic investigations on a masonry bell tower. *Engineering Structures*, 28(5):660 – 667, 2006.
10. S. Ivorra, M. J. Palomo, G. Verdudu, and A. Zasso. Dynamic forces produced by swinging bells. *Meccanica*, 41(1):47–62, 2006.
11. S. Ivorra, F. J. Pallars, and J. M. Adam. Masonry bell towers: dynamic considerations. *Proceedings of the ICE - Structures and Buildings*, 164:3–12(9), 2011.
12. S. Ivorra, F. J. Pallares, and J. M. Adam. Dynamic behaviour of a modern bell tower - a case study. *Engineering Structures*, 31(5):1085 – 1092, 2009.
13. M. Lepidi, V. Gattulli, and D. Foti. Swinging-bell resonances and their cancellation identified by dynamical testing in a modern bell tower. *Engineering Structures*, 31(7):1486 – 1500, 2009.
14. J. Klemenc, A. Rupp, and M. Fajdiga. A study of the dynamics of a clapper-to-bell impact with the application of a simplified finite-element model. *Engineering with Computers*, 27(3):261–272, 2011.
15. J. Klemenc, A. Rupp, and M. Fajdiga. Dynamics of a clapper-to-bell impact. *International Journal of Impact Engineering*, 44(0):29 – 39, 2012.
16. G. Meneghetti and B. Rossi. An analytical model based on lumped parameters for the dynamic analysis of church bells. *Engineering Structures*, 32(10):3363 – 3376, 2010.
17. P. Brzeski, T. Kapitaniak, P. Perlikowski. Experimental verification of a hybrid dynamical model of the church bell. *International Journal of Impact Engineering*, 80):177 –184, 2015.

18. R. Spielmann, A. Rupp, M. Fajdiga, and B. Aztori. Kirchenglocken-kulturgut, musikinstrumente und hochbeanspruchte komponenten. *Glocken-Lebendige Klangzeugen. Schweizerische Eidgenossenschaft, Bundesamt für Kultur BAK.*, pages 22–39, 2008.
19. P. Brzeski, T. Kapitaniak, P. Perlikowski. Analysis of transitions between different ringing schemes of the church bell. submitted to *International Journal of Impact Engineering*.

# Linearization of an invertible bounded iteration in $\mathbb{R}^d$

G. Cirier, LSTA, Paris VI University, France (Email: guy.cirier@gmail.com)

**Abstract.** In this paper, we study an iteration  $f$  in  $\mathbb{R}^d$  defined by a diffeomorphism polynomial bounded. So, the image of the invariant curves is relatively compact and we can use the Fourier-Bohr's representation in the set of almost periodic function ( $A.P.$ ). These curves have asymptotically a parameterization with Weierstrass-Mandelbrot's functions depending on fluctuation's parameters. So, self-similarity and fractal dimension calculus are justified. We apply these results to partial differential calculus.

**Key words:** Bounded invertible iterations, invariant curves, fluctuation's parameters, Weierstrass-Mandelbrot functions, Hénon, Navier-stokes.

## Lead Paragraph

A clear definition of the chaos is a very difficult thing. Mathematically speaking, a chaos is an iteration with a hieratic behaviour, but nobody has a simple mathematical definition. Nevertheless, computing simulations give easily numerous examples. One of the best definition of this situation is the highly sensibility to initial conditions. But this negative definition yields to an impossible long-term prediction. So, each author uses a lot of hypothesis to describe his particular context rendering quite impossible an unified vision of the methods and results. We use here the very restrictive hypothesis of a bounded bijective polynomial iteration in  $\mathbb{R}^d$ . Under this assumption, we obtain a good and general description of the behaviour in terms of series of Weierstrass-Mandelbrot's functions. This approach justifies some methods used by researchers and gives the exact conditions to use it. Another interesting aspect of this method is the possible various generalizations to study more complicate situations.

## 1. Introduction

### A. Definitions and hypothesis

Let  $f$  be an application de  $\mathbb{R}^d$  in  $\mathbb{R}^d$ . We call iteration the same application  $f$  when it is iterated indefinitely:  $f^{(p)}$  with  $f^{(p)} = f \circ f^{(p-1)}$ . We have yet study this problem with probabilistic methods such as the Perron-Frobenius operator [5]. But here,  $f$  is a **polynomial diffeomorphism and applies a bounded set  $C \subset \mathbb{R}^d$  in itself**:  $f(C) \subset C$ . We shall see that the diffeomorphism's hypothesis leads to a deterministic approach.

We recall the definitions of some sets invariant under iterations and H0 hypothesis.

#### 1. Definitions of invariant points or cycles

Let  $f(\mathbf{0}) = \mathbf{0}$  be a fixed point of  $f$  well isolated in  $C$  and  $\lambda$  the eigen values of the linear part of  $f$  at  $\mathbf{0}$ . Iteration of  $f$  induces other invariant points under  $f^{(p)}$ . These points form cycles such as  $f^{(p)}(\alpha) = \alpha$  with  $f(\alpha) \neq \alpha$ . Let  $Fix(f^{(p)})$  this set and  $f_{\bullet}$  the collection of iterations  $f_{\bullet} = (f, f^{(2)}, \dots, f^{(p)} \dots)$ . All that we say about some fixed point  $f(\mathbf{0}) = \mathbf{0}$  will be thru for all the collection  $Fix(f_{\bullet}) = \cup_p Fix(f^{(p)}) \cap C$ .

#### 2. Hypothesis H0

*$f$  is a bounded polynomial diffeomorphism in  $C$ . The eigen values  $\lambda$  of  $f'(\mathbf{0})$  at  $\mathbf{0}$  are **not resonant**:  $1 \neq \lambda^n \mid \forall n \in \mathbb{Z}^d$ . All the  $q < d$  eigen values  $|\lambda| > 1$  are **positive transcendental**.*

If some  $\lambda < -1$  are negative, by iterating  $f$  twice times, we come back in the positive case:  $a(\lambda^2 t) = f \circ f(a(t))$ . So, **we always work with all  $\lambda > 1 \in \mathbb{R}^{+q}$** .

*8<sup>th</sup> CHAOS Conference Proceedings, 26-29 May 2015, Henri Poincaré Institute, Paris France*



## B. Recall of known results for a $C^k$ - diffeomorphism $f$ in $\mathbb{R}^d$ , $k \geq 1$

We consider new invariant sets in our case of a  $C^k$  - diffeomorphism  $f$  in  $\mathbb{R}^d$ ,  $k \geq 1$ : **linearization functions** and **invariant functions**. These functions, quite reciprocal each-others, define **invariant curves** and are well known. They were studied by Steinberg [9]. With Steinberg's series, in the neighbourhood of  $\mathbf{0}$ , we can define  $d$  **linearization  $C^k$  functions**  $\varphi_\ell \circ f(\mathbf{a}) = \lambda_\ell \varphi_\ell(\mathbf{a})$ ,  $\ell = 1, \dots, d$ , under conditions of no resonance. Under the same conditions, we admit that we solve the functional equation  $\mathbf{a}(\lambda \mathbf{t}) = f(\mathbf{a}(\mathbf{t}))$ ,  $\mathbf{t} \in \mathbb{R}^d$  with the Steinberg's series. Then, we get  $d$  **invariant functions**  $\mathbf{a}(\mathbf{t})$ :  $\mathbf{a}_\ell(\lambda \mathbf{t}) = \lambda_\ell \mathbf{a}_\ell(\mathbf{t})$   $\ell = 1, \dots, d$ . More,  $\varphi$  and  $\mathbf{a}$  are unique for a unit Jacobian matrix at  $\mathbf{0}$ .

### 1. The linearization functions $\varphi_\ell(\mathbf{a})$

If  $|\lambda_\ell| < 1$ , then we obtain asymptotically  $\varphi_\ell(\mathbf{a}) = \mathbf{0}$  by iteration of  $f$ . We have a manifold defined by these equations. These results are not very useful here.

### 2. Invariant functions $\mathbf{a}(\mathbf{t})$ and the fluctuation's parameter $\mathbf{t}$

Here, we pay a special attention to  $\mathbf{a}(\mathbf{t})$  constructed with Steinberg's series defined in the neighbourhood of  $\mathbf{0}$ . Let  $\rho > 0$  be the radius of convergence of  $\mathbf{a}(\mathbf{t})$ . Then, taking  $\mathbf{t} : |\mathbf{t}| \leq \rho_0 < \rho$ , we extend  $\mathbf{a}(\lambda^p \mathbf{t}) \in C$  for  $\forall p \in \mathbb{Z}$  with sequential iterations for  $\forall \mathbf{t} \in \mathbb{R}^{+d}$ . This unique solution will be useful. When we iterate of  $f^{(p)}$  with  $p \rightarrow \infty$ , as the coordinates of  $\mathbf{t}$  for  $|\lambda| < 1$  tend to 0, we are only interested by the  $q$  eigen values  $\lambda \in \mathbb{R}^{+q} \parallel \lambda > 1$  and the corresponding  $\mathbf{t} \in \mathbb{R}^{+q}$ .  $\mathbf{t}$  is called **fluctuation's parameter**.

### 3. Remarks

If we start from an arbitrary point  $\mathbf{a}_0 \in C$  and we iterate indefinitely this point, the set obtained, called sometimes orbit, doesn't verify E except if  $\mathbf{a}_0 = \mathbf{a}(\mathbf{t}_0, \mathbf{t}'_0)$ . In this case, iteration verifies asymptotically equation E by continuity. But, we have for each point of  $Fix(f_\bullet)$  curves and invariant measures: we have a « mille-feuilles » of solutions with a well-known very hard complexity. So, if uniqueness of the fixed point  $\mathbf{0}$  in  $C$  is not sure, or if it is not well isolated, we can meet many difficulties. Solutions found here are local.

## C. The problem: find the solutions of the equation E : $\mathbf{a}(\lambda \mathbf{t}) = f(\mathbf{a}(\mathbf{t})) \parallel \lambda > 1, \mathbf{t} \in \mathbb{R}^{+q}$ .

The mean idea of this paper is the following: Under H0, the adherence of the iteration and the invariant function  $\mathbf{a}(\mathbf{t})$  is compact. So, the image of  $\mathbf{a}(\mathbf{t})$  is relatively compact. Then, we can apply the Bohr's results about the almost periodic functions and represent  $\mathbf{a}(\mathbf{t})$  in an almost periodic series. But, equation E implies many conditions on the almost period (a.p.) and on the Fourier's coefficients. Then, we can solve in general the problem in terms of Weierstrass-Mandelbrot functions and obtain a solution. But, as we have say about  $Fix(f_\bullet)$ , if start from an arbitrary point in  $C$ , it is very difficult to describe the convergence to one or to an another set of  $Fix(f_\bullet)$ .

**Here, we search only the unique solution of E (invariant curves corresponding to  $\lambda > 1$ ) in the set of the almost periodic functions (A.P.). We shall see that the solution is also auto similar (A.S.).**

## 2. Bohr's almost periodic functions in a Banach [1] with application to iterations

Let A.P. be the set of the almost periodic functions bounded in  $\mathbb{R}^d$ . Let  $\mathbf{a}(\mathbf{t}), \mathbf{t} \in \mathbb{R}^{+q}, q \leq d$ .

### A. Bochner's definition (recall [2], [3])

A function  $\mathbf{a}(\mathbf{t}) \in A.P.$  in the Bohr's sense, if and only if, the set of the translated functions by all  $\mathbf{c} \{ \mathbf{a}(\mathbf{t} + \mathbf{c}) \mid \mathbf{c}, \mathbf{t} \in \mathbb{R}^{+q} \}$  is relatively compact for the uniform convergence's topology.

Now, we have an arsenal of results near of the Fourier's series [1]. The following theorem 1 is proved in Banach's spaces. Here we use it only in  $\mathbb{R}^d$ .

**B. Theorem 1 (recall of the Bohr's approximation [1])**

Let a trigonometric function:  $P_n(\mathbf{t}) = \sum_{k=1}^n \mathbf{c}_k e^{i\mu_k \mathbf{t}} \in \mathbb{R}^d$  where  $\mu_k, \mathbf{t} \in \mathbb{R}^q$   $\mathbf{c}_k \in \mathbb{R}^d$  and  $\mu_k \mathbf{t}$  is scalar product. If  $\mathbf{a}(\mathbf{t}) \in A.P.$ , we have a sequence of  $P_n(\mathbf{t})$  such as for  $\forall \varepsilon > 0$  :

$$\sup_{\mathbf{t} \in \mathbb{R}^q} \|\mathbf{a}(\mathbf{t}) - P_n(\mathbf{t})\| < \varepsilon.$$

If  $\mathbf{c}(\mu) = \mathbf{F}_\mu(\mathbf{a}) = \lim_{T \rightarrow \infty} \frac{1}{(2T)^q} \int_{-T}^T \dots \int_{-T}^T \mathbf{a}(\mathbf{t}) e^{-i\mu \mathbf{t}} d\mathbf{t}$  is the vector of Fourier-Bohr's coefficients,

then  $\Lambda(\mathbf{a}) = \{\mu \in \mathbb{R}, \mathbf{c}(\mu) \neq \mathbf{0}\}$  is the set of the almost period (a.p.);  $\Lambda$  is countable.  $\mathbf{a}(\mathbf{t})$  is uniformly continuous with Fourier's series:  $\mathbf{a}(\mathbf{t}) \sim \sum_{\mu \in \Lambda} \mathbf{c}(\mu) e^{i\mu \mathbf{t}}$ . This representation is unique.

We have the mean-square convergence and the Parseval's equality.

It is the same to study relative compactness either with  $(\mathbf{t} + \mathbf{c}), \mathbf{t}$ , or  $(\mathbf{t}\mathbf{c})$  where  $\mathbf{c}, \mathbf{t} \in \mathbb{R}^{+q}$  because we can write  $\mathbf{t} + \mathbf{c} = \mathbf{c}'\mathbf{t}, \forall \mathbf{t} \neq \mathbf{0}$ .

**C. Theorem 2**

Under  $H0$ ,  $\{\mathbf{a}(\mathbf{t}), \mathbf{t} \in \mathbb{R}^{+q}\}$  and  $\mathbf{a}(\mathbf{t}\mathbf{c})$  for all  $\mathbf{c}$  are relatively compact and  $\mathbf{a}(\mathbf{t}) \in A.P.$ . Let  $\mathbf{t} = \mathbf{g}(\mathbf{u})$  a  $C^0$  diffeomorphism of  $\mathbb{R}^q$  in  $\mathbb{R}^q$ .  $\mathbf{a} \circ \mathbf{g}(\mathbf{u})$  has again an almost periodic parameterization.

Let  $A_N = \{(\mathbf{a}(\lambda^p \mathbf{t}); \|\mathbf{t}\| \leq \rho_0, p \leq N)\}$ . Its closure  $\hat{A}$  is closed and contained in  $C$  bounded, so is compact. The image of  $\mathbf{a}(\mathbf{t})$  is relatively compact. We « translate »  $\mathbf{t}$  with  $\mathbf{c}$  :  $\mathbf{t}\mathbf{c}$  such as  $\mathbf{a}(\mathbf{t}\mathbf{c}) \in C$ . Let  $n$  be sufficiently large in order to have  $\mathbf{c} = \alpha \lambda^n$  with  $\|\alpha\| < 1$  and  $\|\alpha \mathbf{t}\| < \|\mathbf{t}\| < \rho_0$ ,  $\mathbf{t}\mathbf{c} = \alpha \mathbf{t} \lambda^n$ . As  $f$  is invertible,  $f^{-(n)}(\mathbf{a}(\mathbf{t}\mathbf{c})) = \mathbf{a}(\alpha \mathbf{t})$  with  $\|\alpha \mathbf{t}\| \leq \rho_0$  such as  $A_N$  has adherence  $\hat{A}$ . So  $\mathbf{a}(\mathbf{t}) \in A.P.$ . If  $\mathbf{t} = \mathbf{g}(\mathbf{u})$  a  $C^0$  diffeomorphism of  $\mathbb{R}^q$  in  $\mathbb{R}^q$ , we have again an almost periodic parameterization.

Example:  $\mathbf{g} = (\exp(\mathbf{u}_1), \dots, \exp(\mathbf{u}_q))$  defines the transformation  $\mathbf{u} = \log \mathbf{t}$  and  $\alpha = \log \lambda$  where  $\mathbf{t}, \lambda \in \mathbb{R}^{+q}$ . We can write  $\mathbf{a}(\lambda \mathbf{t}) = \mathbf{a} \circ \exp(\log \lambda \mathbf{t}) = \mathbf{a} \circ \exp(\alpha + \mathbf{u})$  and we have an almost periodic parameterization.

**3. Solution of the equation E:  $\mathbf{a}(\lambda \mathbf{t}) = f(\mathbf{a}(\mathbf{t})), \mathbf{t} \in \mathbb{R}^{+q}$  in  $A.P.$**

As  $\mathbf{a}(\mathbf{t}) \in A.P.$ , we search an asymptotically auto similar solution.

**Definition of an auto similar function**

A function  $\mathbf{w}(\mathbf{t})$  is auto similar if:  $\mathbf{w}(\lambda \mathbf{t}) = r^{-1} \mathbf{w}(\mathbf{t})$  where  $r < 1$  for  $\lambda > 1$  and  $\mathbf{t} \in \mathbb{R}^{+q}$ .

The Weierstrass-Mandelbrot (W-M) function [8]  $w_\lambda(t) = \sum_{k \in \mathbb{Z}} r^k (1 - e^{i\lambda^k t})$  is auto similar where  $r = \lambda^{D-2} < 1$  is the ratio and  $\lambda > 1$  the almost period (a.p.) of  $w$  and  $t \in \mathbb{R}^+$ .

**A. Theorem of linearization 3**

Under  $H0$ , the a.p.  $\mu$  solutions of E are  $\mu = m\lambda^k \mid k \in \mathbb{Z}, m \in \mathbb{N}$  and  $\mathbf{a}(\mathbf{t})$  is written:

$$\mathbf{a}(\mathbf{t}) = \sum_{m \in \mathbb{N}} \mathbf{a}_m(\mathbf{t})$$

with:

$$\mathbf{a}_m(\mathbf{t}) = \sum_{k \in \mathbb{Z}} \mathbf{c}(m\lambda^k) (1 - e^{im\lambda^k \mathbf{t}})$$

If  $m = 1$ ,  $\mathbf{a}_1(\mathbf{t}) = \sum_{k \in \mathbb{Z}} \mathbf{c}(\lambda^k) (1 - e^{i\lambda^k \mathbf{t}})$  is a series of W-M functions  $q$ -dimensional:

$$\mathbf{a}_1(\mathbf{t}) = \sum_{\ell=1}^{\ell=q} \mathbf{c}_\ell w_{\lambda_\ell}(t_\ell)$$

Where:

-  $\mathbf{c}_\ell$  is eigen vector of  $f'(\mathbf{0})\mathbf{c} = \lambda \mathbf{c}$  for the eigen value  $\lambda_\ell > 1$ ,

-  $w_\ell(t)$ , is the one-dimensional W-M function:  $w_\ell(t) = \sum_k r_\ell^k (1 - e^{i\lambda_\ell^k t})$  with  $r_\ell^{-1} = \lambda_\ell^2$ .

But, we denote that  $\mathbf{a}_1(t)$  is not a **solution of E**.

The Taylor's formula of  $f$  in dimension  $d$  is written:  $f(\mathbf{a}) = \sum_{n=0}^{n=n_0} f^n(\mathbf{0})\mathbf{a}^n / n!$ .

Replacing  $\mathbf{a}$  with  $\mathbf{a}(t) \in A.P.$  in the monomials, the equation E implies:

\* for the exponents and the almost period a.p.;

$\sum_j m_j \mu^j - \lambda \mu = 0$  where the integers  $\sum_j m_j \leq n_0$  ( $n_0$  degree of  $f$ ) and  $(\mu^j, \mu)$  are a.p. If  $\mu \in \Lambda(a)$  is an a.p. of  $\mathbf{a}(t)$ , on the one hand,  $\lambda \mu \in \Lambda(a)$  is an a.p., on the other hand,  $m_j \mu \in \Lambda(a)$ . As  $f$  is invertible, all the a.p. are:  $\mu^j = \mu \lambda^k \in \Lambda(a) \mid k \in \mathbb{Z}$ . multiple integers of  $m \mu \in \Lambda(a) \mid m \in \mathbb{N}$ . Then, all the a.p. are:

$$\mu = m \lambda^k = \sum_j m_j \lambda^{kj} \in \Lambda(a) \mid k_j \in \mathbb{Z}$$

But, as  $f$  is polynomial of  $n_0$  degree, the equality on the a.p. contains less than  $n_0 + 1$  terms and a finite condition C can be written:

$$\sum_j m_j \lambda^j - m \lambda^k = 0.$$

Then, as  $\mathbf{a}(t)$  is almost periodic and continue at the origin, we can write:

$$\mathbf{a}(t) = \sum_{m \in \mathbb{N}} (\sum_{k \in \mathbb{Z}} \mathbf{c}(m \lambda^k) (1 - e^{im \lambda^k t}))$$

We observe also that all the integer exponents must be integer multiples of the exponents of the polynomials  $f$ .

\* for the Fourier's coefficients:

The Fourier's coefficients of  $\mathbf{a}(t)$  are obtained Fourier's transformation of  $\mathbf{a}(t)$  for each a.p.  $m \lambda^k$ . So, we apply the Fourier's transformation  $\mathbf{F}_{m \lambda^k}$  to the equation E:

$$\mathbf{c}(m \lambda^{k-1}) / |\lambda| = \mathbf{F}_{m \lambda^k}(\mathbf{a}(t)) \text{ with: } |\lambda| = \prod_{j=1}^{j=q} \lambda_j$$

We can see that  $\mathbf{F}_{m \lambda^k}(\mathbf{a}(t))$  is not easy to compute. We order the computation according to the increasing  $m \in \mathbb{N}$ .

\* First, we consider  $m = 1$ .

The theorem 4 will extend the computation to all  $m$  in particular situations. If  $m = 1$ , condition C becomes:  $\sum_j m_j \lambda^j - \lambda^k = 0$ . If the eigen values  $|\lambda| > 1$  are real positive transcendental, all the coefficients of C must be null:  $m_j = 0 \mid j \neq k$  except  $m_k = 1$ . As  $f$  is polynomial, we study only the transformation  $\mathbf{F}_k(f^{n+m}(\mathbf{0})(a_i(t))^n (a_j(t))^m / n!m!)$  (for the a.p.  $\lambda^k$ ) of a monomial of 2 arbitrary coordinates of  $\mathbf{a}(t) : a_i(t)$  and  $a_j(t)$ . We note:  $\mu_i = \lambda^{s_i}$ . The multinomial formula gives:

$$(a_i(t))^n = n! \sum_{r=1}^d \sum_{\mu} \prod_{p_r=1}^n (c_i(\mu_i))^{p_r} e^{i(\sum p_r \mu_i) t} / p_r!$$

$$(a_j(t))^m = m! \sum_{r=1}^d \sum_{\mu} \prod_{q_s=0}^n (c_j(\mu_j))^{q_s} e^{i(\sum q_s \mu_j) t} / q_s!.$$

The general term  $GT$  of the product is:

$$TG(a_i(t))^n (a_j(t))^m = \sum \prod_{p_r=1}^n c^{p_r} (c_i(\mu_i))^{p_r} \prod_{q_s=0}^n (c_j(\mu_j))^{q_s} e^{i(\sum p_r \mu_i + \sum q_s \mu_j) t}.$$

So, all monomials of degree two or more are null except if :  $\sum p_r \mu_i + \sum q_s \mu_j = \mu_k / \lambda$ . Then:  $i = \ell$  or  $j = \ell$  with  $\mu_i = \mu_k / \lambda$  or  $\mu_j = \mu_k / \lambda$ . All the other coefficients are null. So:

$$\mathbf{F}_k(f^{n+m}(\mathbf{0})(a_i(t))^n (a_j(t))^m / n!m!) = \sum_{\ell=i}^j f'(\mathbf{0}) c_\ell(\mu_k).$$

If  $m = 1$  and if we note  $\mathbf{a}_1(t)$  the solution of E in this case, the previous result means:

$$\mathbf{c}(\lambda^{k-1})/|\lambda| = f'(\mathbf{0})\mathbf{c}(\lambda^k)$$

And,  $\mathbf{c}(\lambda^k)$  is eigen vector of  $f'(\mathbf{0})$  for the eigen values  $\lambda > 1$ . We can write for an eigen value  $\lambda_\ell$  and an eigen vector  $\mathbf{c}_\ell$ :

$$\mathbf{c}_\ell(m\lambda^k) = \alpha_\ell(m\lambda^k)\mathbf{c}_\ell.$$

Then:

$$\alpha_\ell(m\lambda^{k-1})/|\lambda| = \lambda_\ell \alpha_\ell(m\lambda^k)$$

The solution of this recurrence is:  $\alpha_\ell(\lambda^k) = \alpha_\ell r_\ell^k$  with  $r_\ell^{-1} = |\lambda| \lambda_\ell$ .

Then, a coordinate  $\mathbf{a}_{1\ell}(\mathbf{t})$  of  $\mathbf{a}_1(\mathbf{t})$  is:  $\mathbf{a}_{1\ell}(\mathbf{t}) = \mathbf{c}_\ell(\sum_{k \in \mathbb{Z}} \alpha_\ell(\lambda^k)(1 - e^{i\lambda^k t}))$

$$\mathbf{a}_{1\ell}(\mathbf{t}) = \mathbf{c}_\ell \alpha_\ell w_{\lambda_\ell}(\mathbf{t})$$

with  $w_{\lambda_\ell}(\mathbf{t}) = \sum_{k \in \mathbb{Z}} r_\ell^k (1 - e^{i\sum_{j=1}^q \lambda_j^k t_j})$

We must verify the continuity of  $\mathbf{a}_1(\mathbf{t})$  at the origin: if  $t_j = 0 | j \neq \ell$ , we observe that  $F_{\lambda^k}(\mathbf{a}(\lambda\mathbf{t}))$  is now:

$$F_{\lambda^k}(\mathbf{a}(\lambda\mathbf{t})) = \mathbf{c}(m\lambda^{k-1})|\lambda_j|/|\lambda|.$$

To keep the continuity when  $t_j \rightarrow 0$ ,  $\sum_{j=1}^{j=q} \lambda_j^k t_j$  must be reduced to  $\lambda_\ell^k t_\ell$  and  $r_\ell^{-1} = |\lambda_\ell| \lambda_\ell = \lambda_\ell^2$ .

So, the Fourier's transform is reduced to the  $t_\ell$  alone:  $w_{\lambda_\ell}(\mathbf{t}) = w_{\lambda_\ell}(t_\ell)$ .

$$\mathbf{a}_1(\mathbf{t}) = \sum_\ell \mathbf{c}_\ell w_{\lambda_\ell}(t_\ell)$$

We denote that  $\mathbf{a}_1(\mathbf{t})$  is not a **solution of E**: If  $\mathbf{a}_1(\mathbf{t})$  is solution of E, we have:  $\mathbf{a}_1(\lambda\mathbf{t}) = r^{-1}\mathbf{a}_1(\mathbf{t}) = f(\mathbf{a}_1(\mathbf{t}))$  with  $r < 1$ . By iteration, we have:  $\mathbf{a}_1(\mathbf{t}) = \mathbf{0}$ .

#### Remarks:

- If  $\lambda$  is algebraic, the solution is not linear. This case, of null measure, is more difficult because the relations on the coefficients are not linear.
- When we have many eigen values  $\lambda$  greater than the unit, so many  $r < 1$ , we must take  $r_0 = \min r_\ell$ , express all  $r_\ell = r_0^\alpha | \alpha < 1$ , then the process of identification used is quite the same as in the following theorem, but more complicate to present.

We have found a solution  $\mathbf{a}_1(\mathbf{t}) \in A.S.A.P.$ . Now, we construct the general solution  $\mathbf{a}(\mathbf{t}) \in A.S.A.P.$  verifying E: We present here the process of identification when **we have only one eigen value  $\lambda > 1$ , and one ratio  $r < 1$** . We note  $\varepsilon = r^p$  and  $\mathbf{a}_m(\lambda^{-p}\mathbf{t}) = r^{pm}\mathbf{a}_m(\mathbf{t}) = \varepsilon^m \mathbf{a}_m(\mathbf{t})$ . So, we write a priori  $\mathbf{a}(\lambda^{-p}\mathbf{t}) = \sum \varepsilon^k \mathbf{a}_k(\mathbf{t})$ . Let  $g_m(f, A(\mathbf{t})) = \sum_{n=2}^{n=m-1} f^n(\mathbf{0})A_{n,m}(\mathbf{t})$  and  $A_{n,m}(\mathbf{t})$  is polynomial in  $(\mathbf{a}_1(\mathbf{t})\mathbf{a}_2(\mathbf{t})\dots\mathbf{a}_{m-1}(\mathbf{t}))$  such as  $A_{n,m}(\lambda\mathbf{t}) = \varepsilon^m A_{n,m}(\mathbf{t})$ . We proceed by identification gradually. If the process converges, the gap becomes asymptotically null.

#### B. Theorem of recurrence 4

Under  $H0$ , if we have only one eigen value  $\lambda > 1$ , the unique solution of E:  $\mathbf{a}(\mathbf{t}) = \sum \mathbf{a}_m(\mathbf{t}) \in A.S.A.P.$  is obtained with a finite sequence of linear relations with  $\mathbf{a}_1(\mathbf{t})$ :

$$\begin{aligned} (r^{-1} - f'(0))\mathbf{a}_m(\mathbf{t}) &= g_m(f, A(\mathbf{t})) + f^m(\mathbf{0})\mathbf{a}_1(\mathbf{t})^m / m! & \text{if } 2 \leq m \leq n_0, \\ (r^{-1} - f'(0))\mathbf{a}_m(\mathbf{t}) &= g_m(f, A(\mathbf{t})) & \text{if } n_0 + 1 \leq m \leq n_0^2, \end{aligned}$$

We take advantage of the function  $\mathbf{a}_1(\mathbf{t})$ , by observing that the invariant functions are asymptotically tangential to the eigen vectors at  $\mathbf{0}$  and  $\mathbf{a}_\infty(\mathbf{t})$  are these asymptotes.

With  $\varepsilon = r^p$ , equation E is:

$$\mathbf{a}(\lambda^{-p+1}\mathbf{t}) = f(\mathbf{a}(\lambda^{-p}\mathbf{t})) = r^{-1}(\sum_{m=1}^{m=N} \varepsilon^m \mathbf{a}_m(\mathbf{t})) = f(\sum_{m=1}^{m=N} \varepsilon^m \mathbf{a}_m(\mathbf{t})).$$

We order  $f(\sum \varepsilon^m \mathbf{a}_m(\mathbf{t}))$  according to the power of  $\varepsilon : f(\sum_{m=1}^N \varepsilon^m \mathbf{a}_m(\mathbf{t})) = \sum_{m=1}^{N_0} \varepsilon^m g_m(\mathbf{a}(\mathbf{t}))$  with a finite  $N$  because  $f$  is polynomial. We identify all the coefficients of  $\varepsilon$ . The recurrence begins with  $(r^{-1} - f'(0))\mathbf{a}_1(\mathbf{t}) = 0$  where  $\mathbf{a}_\infty(\mathbf{t}) = \mathbf{a}_1(\mathbf{t})$  belongs to *A.S.A.P.* Then, we have easily  $(r^{-1} - f'(0))\mathbf{a}_2(\mathbf{t}) = f''(0)\mathbf{a}_1(\mathbf{t})^2 / 2!$  which verifies the recurrence. And so on. We observe that  $g_k$  are polynomials in  $(\mathbf{a}_1(\mathbf{t}), \mathbf{a}_2(\mathbf{t}), \dots, \mathbf{a}_{k-1}(\mathbf{t}))$  such as  $A_{n,m}(\lambda) = \varepsilon^m A_{n,m}(\mathbf{t})$ . Degree of  $f$  being  $n_0$ , the process of identification stop for  $N = n_0$ .

So, the knowledge of  $\mathbf{a}_1(\mathbf{t})$  corresponding to  $\lambda > 1$  determines completely  $\mathbf{a}(\mathbf{t})$ .

### C. Corollary 2

Under the previous hypothesis, if  $\lambda > 1$ ,  $D = 0$  and if  $\lambda < -1$ ,  $D = 1, 25$ . If  $g = f^{(p)}$  and if  $\lambda(g) > 1$ ,  $r_\ell^{-p} = \lambda_\ell^{1+1/p}$  and  $D = 2 - 1/p - 1/p^2$ .

Now, we calculate the dimension  $D$  of each coordinate of the asymptotic solution. The dimension's formula (with the box method) is for WM ( $D = 2 + \log|r_0| / \log|\lambda|$ ).

If  $\lambda > 1$ , then  $r^{-1} = \lambda^2$  and  $D = 0$ , we have points only. If  $\lambda < 0$ , iterating  $f$  twice times, we get  $g = f \circ f$ . If  $g$  has the eigen values  $\lambda > 1$ , then  $r^{-2} = \lambda\sqrt{\lambda} = \lambda^{3/2}$ . So:  $D = 2 + \log \lambda^{-3/4} / \log \lambda = 2 - 0,75$  et  $D = 1,25$ .

If  $g = f^{(p)}$  and if  $g$  has the eigen values  $\lambda_\ell > 1$ ,  $f$  has the eigen values  $\lambda_\ell^{1/p}$ , and the a.p. of  $f$  is  $\lambda_\ell^{1/p}$ . If  $r_\ell$  is the ratio of  $f$ ,  $r_\ell^p$  is the ratio of  $g$ . The recurrence  $c(\mu \lambda_\ell^{1/p}) / \lambda_\ell^{1/p} = \lambda_\ell c(\mu)$  of  $g$  implies  $r_\ell^{-p} \lambda_\ell^{-1/p} = \lambda_\ell$ .

### D. Consequences

#### 1. Mathematical

- If  $\lambda = \rho e^{i\theta}$  with  $\theta = 2k\pi / p$ , iterating  $f^{(p)}$ ,  $\lambda^p = \rho^p > 1$ , we meet the same conditions of the corollary and the dimension is:  $D = 2 - (p+1)/p^2$ . We are leading to same situation as for cycles of order  $p$ .  $g = f^{(p)}$  leaves invariant each point of the cycle. Invariant curves are tied to each point of cycle as previously. The solution is cyclic

- More generally, if the eigen values are complexes,  $\lambda = \rho e^{i\theta}$ , we can approximate  $\theta$  with Dirichlet by  $\theta \sim 2k\pi / p$ , but we must verify the continuity of the solution with  $\theta$ .

- We can replace polynomials  $f$  by analytical functions (Favard [7]) without changes of results: if  $f$  is diffeomorphism  $C^\infty$ , interior of a disk de convergence  $\|\mathbf{a}\| < \rho_1$ ,  $f$  is uniformly approximated by polynomial. Then, taking  $\mathbf{t}$  sufficiently small, we keep the results.

- Many problems remain when we have many fixed points.

#### 2. Methodological

We give a mathematical justification of the methods used by physicists :

- As the almost periodic function tends asymptotically to a WM's function, the use of the auto similarity is justified, with the methods of fractal dimension. We can use also auto correlation(s) function.

- The sensitivity to initial conditions does not modify the global shape of the curves. The « thru » chaos results from the WM's functions.

- If we can give the global shape of the curve, we are unable to situate exactly a point on the curve at any time.

A fixed point seems to define the solution. But, if we have fixed many points in  $C$ , we have observed possibilities of passage from a domain near a fixed point to another.

#### Example : case of bounded Hénon

This iteration is defined in  $\mathbb{R}^2$  by

$(a_1, b_1) = (\gamma a + b + h(a), \beta a)$  where  $\gamma = \lambda + \lambda'$  and  $\beta = -\lambda\lambda'$  with  $|\lambda| > 1$  and  $|\lambda'| < 1$ . Its invariant curve is  $\mathbf{a}(t) = (a(\lambda t), a(t))$  verifying:  $a(\lambda t) = \gamma a(t) + \beta a(t/\lambda) + h(a(t))$ .

If  $\lambda$  is negative, with 2 iterations, we are in the positive case. But, we have to study the recurrence of the twice times itered function and we have cycles of order 2 instead of fixed points and we have a fractal situation. We get :

$$(a_2, b_2) = (\gamma(\gamma a + b + h(a)) + \beta(\gamma a + b + h(a)) + h(\gamma a + b + h(a)), \beta(\gamma a + b + h(a)))$$

The eigen values greater than 1 is now  $\lambda^2$ . But we can have complexes roots or resonance.

**Nota :** In the classical Hénon's iteration, we have  $h(a) = -\sigma a^2$  with  $\sigma = 1, 4$ ,  $\beta = 0, 3$  and  $\gamma = -2\sigma * 0,6313 = -1,7678$ . Eigen values at the fixed point 0 are  $\lambda \approx -1,9237$  and  $\lambda' \approx 0,1559$ . They are algebraic, and the theory can't be apply.

Nevertheless, if we apply it: the curve  $(a, b) = (a(t\lambda), a(t))$  defined by  $a(\lambda^2 t) = a(t) / r = w_r(t) / r$  is: either  $(1 - r\beta)a(t\lambda) = \gamma a(t) + h(a(t))$ , or  $(1 - r\beta)a(t) / r = \gamma a(t\lambda) + h(a(t\lambda))$ . This last formula induces many branches that we can approximate.

#### 4. Property P of the W-M function and resonance

Now, we speak about an interesting property of the W-M function  $w_\lambda(t) = \sum_{k \in \mathbb{Z}} r^k (1 - e^{i\lambda^k t})$ . As usual, we write the ratio  $r$  as a fixed function of  $\lambda$ :  $r = \lambda^{2-D}$ .

##### A. Lemma

The W-M function verifies for  $\forall p, q \in \mathbb{N}$  the property P:

$$w_\lambda(t) = (p/q) w_{\lambda^{p/q}}(t)$$

When we write  $k = np + \alpha$  with  $\alpha = 0, 1, 2, \dots, n-1$  and  $p \in \mathbb{Z}$ , we have:

$$\begin{aligned} w_\lambda(t) &= \sum_{p \in \mathbb{Z}} \sum_{\alpha=0}^{\alpha=n-1} r^{np+\alpha} (1 - e^{i\lambda^{np+\alpha} t}) = \sum_{\alpha=0}^{\alpha=n-1} r^\alpha \sum_{p \in \mathbb{Z}} r^{np} (1 - e^{i\lambda^{np} (\lambda^\alpha t)}) \\ &= \sum_{\alpha=0}^{\alpha=n-1} r^\alpha w_{\lambda^n}(\lambda^\alpha t) = n \sum_{p \in \mathbb{Z}} r^{np} (1 - e^{i\lambda^{np} t}) = n w_{\lambda^n}(t) \end{aligned}$$

As we have  $w_\lambda(t) = n w_{\lambda^n}(t)$  for  $n \in \mathbb{N}$ , then the relation is thru for all fraction  $p/q$ .

##### B. "Continuity" with $\lambda$

In general,  $w_\lambda(t)$  is not a continuous function of  $\lambda$ .

But, on the set  $S_\lambda = \{\lambda^{p/q} | p, q \in \mathbb{N}\}$ ,  $w_{\lambda^{p/q}}(t)$  presents a kind of continuity in the sense:

As  $w_{\lambda^{p/q}}(t) - w_\lambda(t) = (q/p - 1)w_\lambda(t)$ , then we have:  $w_{\lambda^{p/q}}(t) - w_\lambda(t) \rightarrow 0$  when  $q/p \rightarrow 1$ .

##### C. Resonance

To study the resonance, we have to consider, for  $\forall t \in \mathbb{R}^{+d}$  instead of  $\forall t \in \mathbb{R}^{+q}$ , the invariant function  $\mathbf{a}(t)$  and find the solution of the equation E:  $\mathbf{a}(\lambda t) = f(\mathbf{a}(t))$ ,  $t \in \mathbb{R}^{+d}$ . Then, under H0, we search the asymptotic solution when we iterate  $f$  indefinitely. All the previous results of part II remain thru if all the eigen values are positive transcendental and no resonant. So, we study only the linear part  $\mathbf{a}_1(t)$  of  $\mathbf{a}(t)$  represented by W-M functions.

We begin to solve the case with two eigen values  $\lambda$  and  $\lambda_1$  such as  $\lambda_1 = \lambda^{\varepsilon p/q}$  where  $\varepsilon = \pm 1$ . In this case, we can write explicitly:  $\mathbf{a}_1(t) = \mathbf{a}_{\lambda, \lambda^{\varepsilon p/q}}(t, t_1)$  in words of W-M functions. Each coordinates of  $\mathbf{a}_{\lambda, \lambda^{\varepsilon p/q}}(t, t_1)$  corresponding to  $\lambda$  and  $\lambda_1$  can be written as:  $a_{\lambda, \lambda^{\varepsilon p/q}}(t, t_1) = c w_{\lambda, \lambda^{\varepsilon p/q}}(t, t_1) = c \sum_{k \in \mathbb{Z}} r^k (1 - e^{i(\lambda^k t + \lambda^{\varepsilon p/q} t_1)})$

##### D. Proposition

If  $\varepsilon = +1$ , then  $\mathbf{a}_{\lambda, \lambda^{p/q}}(t, t_1) = \mathbf{a}_{\lambda^{p/q}}(t + t_1)$ ,

If  $\varepsilon = -1$ , we have a resonance, then:  $\mathbf{a}_1(t, 0) = \mathbf{a}_1(\lambda^{p/q-1}t, 0)$

More generally, if  $\lambda_1^p \lambda^n = 1$  with  $|\lambda_1| < 1$  and  $|\lambda| > 1$ ,  $\lambda \in \mathbb{R}^q$ , we have  $\mathbf{a}_1(t, 0) = \mathbf{a}_1(\lambda^{n-1}t, 0)$ .

If  $\varepsilon = +1$ , we have for the coordinates  $(t, t_1)$  corresponding to  $(\lambda, \lambda_1)$ :

$$w_{\lambda, \lambda^{p/q}}(t, t_1) = (q/p)w_{\lambda, \lambda}(t, t_1) = (q/p)\sum_{k \in \mathbb{Z}} r^k (1 - e^{i\lambda^k(t+t_1)}) = (q/p)w_{\lambda}(t+t_1) = w_{\lambda^{p/q}}(t+t_1).$$

If  $\varepsilon = -1$ , we have a resonance.

We can take any  $\lambda'_1 \in S_{\lambda}$  very near to  $\lambda_1$  such as  $\lambda'_1{}^\gamma \lambda \neq 1$ , with  $\gamma = p'/q' \rightarrow p/q$  and  $p', q' \in \mathbb{N} | p'/q' \neq p/q$ . As  $(\lambda, \lambda'_1)$  is not resonant, by iterating  $f$ , we get asymptotically:

$$\mathbf{a}_{\lambda, \lambda'_1}(t, 0) = \lim_{t_1 \rightarrow 0} \mathbf{a}_{\lambda, \lambda'_1}(t, t_1) \text{ for the a.p. } \lambda. \text{ Then: } \mathbf{a}_{\lambda, \lambda_1}(t, 0) = \lim_{\lambda'_1 \rightarrow \lambda_1 \in S_{\lambda}} \mathbf{a}_{\lambda, \lambda'_1}(t, 0). \text{ We have:}$$

$$w_{\lambda, \lambda^{-p/q}}(t, t_1) = (q/p)w_{\lambda, \lambda^{-1}}(t, t_1) = (q/p)\sum_{k \in \mathbb{Z}} r^k (1 - e^{i(\lambda^k t + \lambda^{-k} t_1)}) = \sum_{k \in \mathbb{Z}} r^k (1 - e^{i(\lambda^{kp/q} t + \lambda^{-k} t_1)}) \\ = w_{\lambda^{p/q}, \lambda}(t, t_1)$$

Iterating  $f$  indefinitely, the asymptotic is also  $\mathbf{a}_1(t, 0) = \lim_{t_1 \rightarrow 0} \mathbf{a}_1(t, t_1)$  for the a.p.  $\lambda^{p/q}$ .

Iterating  $f$  one time the equation E, we have  $\mathbf{a}_1(\lambda t, 0) = \mathbf{a}_1(\lambda^{p/q} t, 0)$ . Then:  $\mathbf{a}_1(t, 0) = \mathbf{a}_1(\lambda^{p/q-1} t, 0)$ .

If  $\lambda_1^p \lambda^n = 1$  with  $|\lambda_1| < 1$  and  $|\lambda| > 1$ ,  $\lambda \in \mathbb{R}^q$ ,  $\mathbf{a}_1(t)$  verifies:

$$\mathbf{a}(t/\lambda, t'/\lambda) = f'(\mathbf{0})\mathbf{a}(t, t'). \text{ Let } |n||q| = \prod_{j=1}^{i=q} n_j \prod_{j=q+1}^{i=d} q_j. \text{ We can multiply the equation by } |n||q|: |n||q|\mathbf{a}_{\lambda, \lambda'}(t/\lambda, t'/\lambda) = |n||q|f'(\mathbf{0})\mathbf{a}_{\lambda, \lambda'}(t, t'). \text{ That means that we change } \lambda \text{ in } \lambda^n \text{ and } \lambda' \text{ in } \lambda'^q: \mathbf{a}_{\lambda^n, \lambda'^q}(t/\lambda^n, t'/\lambda'^q) = f'(\mathbf{0})\mathbf{a}_{\lambda^n, \lambda'^q}(t, t'). \text{ Uniqueness implies: } \mathbf{a}_1(t, 0) = \mathbf{a}_1(\lambda^{n-1}t, 0).$$

## 5. Conclusion

This study is based on the fact that  $f$  is biunivoque. In other cases, the probabilistic methods previously used [5] must be applied to the iterations with multiple inverses.

But, if the number  $m$  of inverses of  $f$  is finite, we can randomly draw each inverse branch with a probability  $1/m$ . Then, the WM's functions can be easily randomised.

Besides, the set of the WM's functions contains some stochastic processes.

## References

- [1] Amerio, Prouse, 1971. *Almost Periodic Functions and Functional Equations*, Van Nostrand.
- [2] Bochner S., 1925. *Sur les fonction presque périodiques de Bohr*, CR, t 177, p737.
- [3] Bohr H., 1923. *Sur les fonctions presque périodiques*, CR, t 180, p1156.
- [4] Cirier G., 2005. *Solution stationnaire de l'équation associée à un opérateur de Perron- Frobenius dans le cas de difféomorphismes à point fixe*, Ann. ISUP, Vol. XLIX, Fasc 1, p35.
- [5] Cirier G., 2012. *Probabilistic and asymptotic methods*. hal-00691097, v. 3.
- [6] Cirier G., 2014. <https://hal.archives-ouvertes.fr/hal-01053416v4/document>
- [7] Favard J., 1927. *Sur les fonctions harmoniques presque périodiques*. Thèse. Numdam.org
- [8] B.B. Mandelbrot, *Fractals: Forms, Chance and Dimension*, Freeman, 1977.
- [9] Steinberg S., 1958. *On the structure of local homeomorphisms of Euclidian n-space*. A.J.M. 80.3.

## Appendix 1. Application to partial differential equations

We consider the differential equation:

$$\partial \mathbf{a} / \partial \mathbf{x} = F(\mathbf{a}).$$

The unknown functions are a vector  $\mathbf{a} \in \mathbb{R}^d$ . The variable is  $\mathbf{x} \in \mathbb{R}^{d+}$ .  $F(\mathbf{a})$  is a matrix  $(d, d)$  of

polynomials of  $\mathbf{a} \in \mathbb{R}^d$  in  $\mathbb{R}^d$ . With no lack of generality, we can take equal so many coordinates of  $\mathbf{x}$  as we want. If all coordinates are equal with one  $x$ , we have an ODE. See Arnold [1]. First, we translate this differential equation in words of iteration.

## 1. Generalities

### 1. Notations

We call differential iteration  $f(\mathbf{a}, \delta)$  of  $\mathbb{R}^d$  in  $\mathbb{R}^d$  the function defined as:

$$\mathbf{a}_1 = f(\mathbf{a}, \delta) = \mathbf{a} + \delta F(\mathbf{a}), \text{ with } \delta \in \Delta = \mathbb{R}^{d+} \cap \{\delta_0 \geq \delta \geq 0\}.$$

As usual, we link  $\delta$  to  $\mathbf{x}$  with  $\delta = \mathbf{x} / n$ ,  $n \in \mathbb{N}$ ,  $\mathbf{x} \in \mathbb{R}^d$ . We note  $\mathbf{x}F = x_\ell F_\ell \mid \ell = 1, \dots, d$ .

If  $F(\boldsymbol{\alpha}) = \mathbf{0}$ ,  $\boldsymbol{\alpha}$  is a fixed point of the iteration  $f(\mathbf{a}, \delta)$ ;  $\boldsymbol{\alpha}$  doesn't depend on  $\delta \in \Delta$ . If  $\rho$  is an eigen value of  $F'(\boldsymbol{\alpha})$ , then  $\lambda = 1 + \mathbf{x}\rho / n$  is eigen value of  $f(\mathbf{a}, \delta)$ .

For all small  $\delta \leq \delta_0$ ,  $f(\mathbf{a}, \delta)$  is invertible in a neighbourhood of the fixed point  $\mathbf{0}$ ; then,  $f(\mathbf{a}, \delta)$  is a  $C^\infty$  diffeomorphism. The iteration can be written in the basis of the eigen vectors of  $\partial F(\boldsymbol{\alpha}) / \partial \mathbf{a}$ . In this basis, we write:  $f_\ell(\mathbf{a}, \delta) = (1 + \delta_\ell \rho_\ell) a_\ell + \delta_\ell G_\ell(\mathbf{a})$ ,  $\ell = 1, \dots, d$  where  $G_\ell(\mathbf{a})$  is polynomial with a term of lowest degree  $\geq 2$ .

We study the differential iteration only for  $m = 1$  as in theorem 3. We rewrite H0:

### 2. Hypothesis 1

For all  $\delta \in \Delta$ ,  $f(\mathbf{a}, \delta)$  applies a bounded set  $C$  of  $\mathbb{R}^d$  in itself. We have  $q$  transcendental eigen values  $\rho_\ell > 0$ , all the others are negative. Then:  $\lambda_\ell = 1 + \mathbf{x}_\ell \rho_\ell / n > 1$ .

With the Steinberg series, we define  $d$  invariant functions  $\mathbf{a}(\mathbf{u})$  with the equation **E**:

$$a_\ell(\lambda \mathbf{u}) = f_\ell(\mathbf{a}(\mathbf{u}), \delta) \quad \ell = 1, \dots, d$$

By iteration  $f^{(p)}(\mathbf{a}, \delta)$ , we extend, beyond the disk of convergence, the definition of  $f(\mathbf{a}(\mathbf{u}), \delta)$  for  $\mathbf{u} \in \mathbb{R}^d$ .  $\mathbf{u} \in \mathbb{R}^q$  is called the fluctuation's parameter.

## 2. Proposition 4

Under H1, the equation **E**:  $\mathbf{a}(\lambda \mathbf{u}) = f(\mathbf{a}(\mathbf{u}), \delta)$  of the differential iteration has an asymptotic almost periodic solution.

The a.p. are  $\boldsymbol{\mu} = m(1 + \delta \rho)^k \mid k \in \mathbb{Z}, m \in \mathbb{N}$ . We can write

$$\mathbf{a}(\mathbf{u}) = \sum_{m \in \mathbb{N}} \mathbf{a}_m(\mathbf{u})$$

with

$$\mathbf{a}_m(\mathbf{u}) = \sum_{k \in \mathbb{Z}} \mathbf{c}(m \lambda^k) (1 - e^{im \lambda^k \mathbf{u}})$$

For  $m = 1$ ,  $\boldsymbol{\mu}_k = \lambda^k$ , the coefficients  $\mathbf{c}(\boldsymbol{\mu}_k)$  verify:

$$\mathbf{c}_\ell((1 + \delta \rho)^k) = (1 + \delta_\ell \rho_\ell)^{-2k} \mathbf{c}_\ell$$

where  $\mathbf{c}_\ell$  be the eigen vector of  $\partial F(\boldsymbol{\alpha}) / \partial \mathbf{a}$  for the eigen values  $\rho_\ell > 0$ .

When  $n \rightarrow \infty$ :  $\mathbf{a}_1(\mathbf{u}) = \mathbf{c} \sum_{k \in \mathbb{Z}} \lambda^{-2k} (1 - e^{i \lambda^k \mathbf{u}}) = \mathbf{c} \mathbf{w}_r(\mathbf{u})$  and  $\lambda_\ell = e^{x_\ell \rho_\ell}$ .

where  $\mathbf{w}_r(\mathbf{u}_\ell)$  is the WM's functions with  $\lambda_\ell = \exp(x_\ell \rho_\ell)$  and  $r_{r_0, \ell} = (\lambda_\ell)^{-2} = \exp(-2x_\ell \rho_\ell)$ .

Let  $\hat{S}_{\delta_0}$  be the adherence of  $f^{(p)}(\mathbf{a}(\mathbf{u}), \delta)$  for all  $\delta \in \Delta$  when  $p \rightarrow \infty$ .  $\hat{S}_{\delta_0}$  is closed and bounded, so  $\hat{S}_{\delta_0}$  is compact.  $f(\mathbf{a}(\mathbf{u}), \delta)$  is uniformly continue for all  $\delta \in \Delta$ . When  $p \rightarrow \infty$ , all the coordinates of  $\mathbf{u}$  corresponding to  $\rho_\ell < 0$   $\mathbf{u}$  tend to 0. We denote  $\mathbf{u}$  the vector corresponding to the eigen values  $\rho_\ell > 0$ . this variable is called fluctuation.

We get a representation of  $f(\mathbf{a}(\mathbf{u}), \delta)$  by almost periodical functions and we develop  $\mathbf{a}(\mathbf{u})$  with Fourier's series:  $\mathbf{a}(\mathbf{u}) \sim \sum_{\mu \in \Lambda} \mathbf{c}(\mu) e^{i\mu u}$ . The set of the a.p.  $\Lambda(\mathbf{a}) = \{\mu \in \mathbb{R}, \mathbf{c}(\mu) \neq 0\}$  is countable. We apply the previous results of theorem 3:

The  $q$  eigen values  $\rho_\ell > 0$  get the a.p.  $\mu = m(1 + \delta\rho)^k \mid k \in \mathbb{Z}, m \in \mathbb{N}$ . So, we recall:

$$\mathbf{a}(\mathbf{u}) = \sum_{m \in \mathbb{N}} \mathbf{a}_m(\mathbf{u})$$

and:

$$\mathbf{a}_m(\mathbf{u}) = \sum_{k \in \mathbb{Z}} \mathbf{c}(m\lambda^k) (1 - e^{im\lambda^k u})$$

We continue the computation of the coefficients  $\mathbf{c}(\mu_k)$  for  $m = 1$  under the hypothesis that the  $\delta\rho$  are transcendental. Let  $\mathbf{c}$  be the eigen vector of  $\partial F(\alpha) / \partial \mathbf{a}$  for the eigen values  $\rho_\ell > 0$ . The equation E becomes:

$$\mathbf{c}_\ell ((1 + \delta\rho)^{k-1}) = (1 + \delta_\ell \rho_\ell)^2 \mathbf{c}_\ell ((1 + \delta\rho)^k)$$

Then:

$$\mathbf{c}_\ell ((1 + \delta\rho)^k) = (1 + \delta_\ell \rho_\ell)^{-2k} \mathbf{c}_\ell$$

And:  $\mathbf{a}_1(\mathbf{u}) = \mathbf{c} \sum_{k \in \mathbb{Z}} \lambda^{-2k} (1 - e^{i\lambda^k u}) = \mathbf{c} \mathbf{w}_r(\mathbf{u})$  with  $\mathbf{r} = \lambda^{-2}$ . We observe that  $\lambda_\ell = (1 + \delta_\ell x_\ell / n)$ . With the property II-8 of W-M function, when we take  $\lambda_\ell^n \mid n \in \mathbb{N}$  instead of  $\lambda_\ell$ ,  $w_r(t) = n w_{r^n}(t)$ . Then:  $\lambda_\ell^n = (1 + \delta_\ell x_\ell / n)^n \rightarrow \exp(\delta_\ell x_\ell)$  and  $r_\ell = \exp(-2x_\ell \rho_\ell)$ .

### 3. Remarks

- If we have many fixed points in  $C$ , we observe the possibility of passages of a domain of a fixed point to another.

- The equation of Navier Stokes [2] is written as  $\partial \mathbf{a} / \partial \mathbf{x} = F(\mathbf{a})$ . Initially we have  $n + 1$  unknown variables  $(u, p)$  with so many variables  $(\mathbf{x}, t)$  and differential equations. We note  $\partial u_i / \partial \mathbf{x} = \mathbf{b}_i$ ,  $i = 1, \dots, n$   $\Delta u_i = \sum_{j=1}^n \partial^2 u_i / \partial x_j^2 = \sum_{j=1}^n \partial \mathbf{b}_i / \partial x_j$ ,  $\mathbf{c} = (\mathbf{x}, t)$   $d_i = \partial p / \partial x_i$ . Then :

$$\partial \mathbf{u} / \partial t + \sum_{j=1}^n u_j \mathbf{b}_{ij} = \nu \sum_{j=1}^n \partial \mathbf{b}_i / \partial x_j - d_i + f_i(\mathbf{c})$$

$$\sum_{j=1}^n \partial u_j / \partial x_j = 0, \quad \partial u_i / \partial \mathbf{x} = \mathbf{b}_i, \quad i = 1, \dots, n, \quad \mathbf{c} = (\mathbf{x}, t)$$

If the outer forces  $f_i$  are polynomial and the differential iteration bounded, then the solution will be almost periodic as we have seen. If it is difficult to find periodic solutions [2], on the other hand, the almost periodic functions solve the question. The Lorenz's attractor gives the proof. The difficulty doesn't come from differential operators which are quadratic for the iteration, but from the  $f_i$ .

- With the same methods, we can study iterations with decay:  $\mathbf{u}_1(\mathbf{x}) = F(\mathbf{u}(\mathbf{x} + \mathbf{T}))$ : if  $\mathbf{T} = \log(\tau)$ ,  $\mathbf{x} = \log(t / \tau)$  and  $\mathbf{a}(t) = \mathbf{u} \circ \log(t)$ , we have  $\mathbf{a}_1(t / \tau) = F(\mathbf{a}(t))$ , then  $(\lambda / \tau)$  take place of  $\lambda$ .

### References

[1] Arnold V., *Chapitres supplémentaires de la théorie des EDO*. Mir, Moscou 1980.

[2] Fefferman C. L., [http://www.claymath.org/millennium/Navier-Stokes\\_Equations/navierstokes.pdf](http://www.claymath.org/millennium/Navier-Stokes_Equations/navierstokes.pdf)